W.L. Smith

WBG-1

Department of Meterorology
The University of Wisconsin
June, 1962

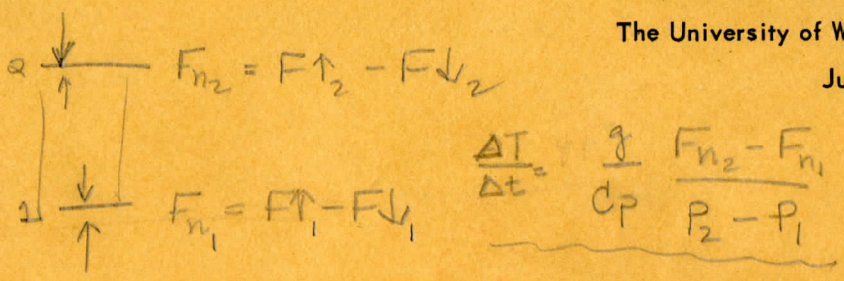

INFRARED RADIATION MEASUREMENTS IN THE ATMOSPHERE

Annual Report
WBG-1

The research reported in this document has been sponsored by the Office of Meteorological Research, U.S. Weather Bureau, Director, Dr. Harry Wexler.

RADIOMETERSONDE OBSERVATIONS OF WATER VAPOR FLUX EMISSIVITY

BY

P. M. KUHN

U. S. Weather Bureau, Dept. of Meterorology,
University of Wisconsin

ABSTRACT

Employing two hundred and eleven nocturnal radiometersonde observations of upward infrared flux, air temperature, and relative humidity in the atmosphere the water vapor flux emissivity as a function of optical depth has been determined. The principle results of this study are:

(a). A new curve of water vapor flux emissivity, obtained from "in situ" atmospheric measurements, is compared with previous work. The emissivities are most reliable for optical depths typical of the troposphere as most of the data was obtained in those levels. One low stratospheric ascent made possible the measurement of a few values at low pressure and very shallow optical depth.

(b). When calculating infrared radiative flux in the atmosphere from temperature, humidity and pressure data, the accuracy will be improved if a pressure reduced optical depth of $(p/p_o)^{.85}$ is used.

(c). There is evidence that a single pressure reduced optical depth ratio will not serve over a wide range of optical depths, including both the stratosphere and troposphere. But no further work would be profitable until more stratospheric ascents at very shallow optical depths are available.

List of Figures

TABLE OF SYMBOLS

(Listed in order introduced)

Symbol	Meaning	First used in equation number
$\epsilon f(u)$	Flux emissivity	1.1
v	Optical depth of gas in precipitable centimeters	1.1
$F(u,T)$	Infrared flux	1.1
T	Temperature	1.1
F_b	Black body flux	1.1
σ	Boltzmann Constant ($.817 \times 10^{-10}$ cgs)	1.2
$\bar{q}$	Mean specific humidity	1.2
p	Pressure	1.2
g	Acceleration due to gravity (c.g.s.)	1.2
$F_r(u,T)$	Infrared flux at reference level	1.5
$\bar{T}$	Mean temperature of atmospheric layer	1.5
$(u)_w$	Optical depth of water vapor (pr. cm.)	3.1
$(u)_c$	" " " carbon dioxide (pr. cm.)	3.1
$(u)_o$	" " ozone (pr. cm.)	3.1
i	Indexing variable	3.1
$\Delta\epsilon$	Finite increment of flux emissivity	3.1
T_o	Interface radiative equilibrium temperature	3.1
ν	Indexing variable	3.2
$F_o\uparrow$	Observed upward infrared flux	3.2
A	Constant equal to a_o	4.1
$\bar{a}_o$	Constant in polynomial expansion	4.1

Symbol	Meaning	First used in equation number
a_1	Constant in polynomial expansion	4.1
a_n	" " " "	4.1
S.E.	Unbiased standard error	4.2
y_i	Polynomial variable	4.2
$\bar{y}_i$	Mean value for polynomial variable	4.2
$\hat{y}$	$y_i - y$	4.2
N	Total number of variables	4.2
$F_\lambda(T)$	Spectral flux	4.3
$L_\lambda(v)$	Elsasser's generalized absorption coefficient	4.3
	wavelength	4.4
k_λ	Distribution of absorption	4.4
x	Half width of Lorentz line shape	4.4
λ_o	Wave length at standard pressure and temperature	4.4
α_o	Line half width at standard pressure and temperature	4.5
T_o	Surface temperature	4.5
p_o	Surface pressure	4.5
A_λ	Spectral absorption	4.6
χ	Variable equal to $3u/2\pi\alpha$	4.6
e	Exponential notation (base e)	4.6
	order	
J_o	Zeroth Bessel function	4.6
J_1	1st order Bessel function	4.6
i	Imaginary number symbol	4.6
$F(x)$	Functional notation	4.6
v^*	Exponent of pressure ratio	4.9
γ	Reduced optical depth	4.9
T_b	Bottom radiometer sensor temperature	A1
a	Absorptivity	A1

Symbol	Meaning	First used in equation number
L	1.0 band transmissivity of polyethylene film	A1
k_i	Internal thermal conductivity of air	A1
T_t	Top radiometer sensor temperature	A1
Δz_i	Internal cell thickness of radiometer	A1
k_b	Bottom thermal conductivity of air	A1
T_a	Air temperature	A1
Δz_b	Bottom cell thickness of radiometer	A1
λ	Product of effective specific heat and effective mass/cm of radiometer sensor	A1
t	Time	A1
σ'	Root mean square deviation (r.m.s. deviation)	A2

1. Introduction

The availability of numerous direct radiometersonde measurements of atmospheric infrared flux under nocturnal cloudless conditions in the free atmosphere has made possible "in situ" measurements of water vapor flux or slab emissivity. Such measurements have been made with the airborne radiometersonde (Suomi and Kuhn, 1958). The purpose of this study is to determine water vapor flux emissivity and its pressure dependence as a function of optical depth and pressure using direct radiometersonde observations of infrared flux and to compare these measurements with existing laboratory and free air measurements.

Flux Emissivity

Flux or slab emissivity is defined as the ratio of infrared (hereafter termed "IR") flux to black body flux at the same temperature and is given by:

$$\epsilon_f(u) = F(u,T)/F_b \qquad (1.1)$$

Eq (1.1) applies separately to each gaseous absorber in the atmosphere. The following is the development of an expression for the computation of IR flux at any level in the atmosphere by the method of isothermal emissivities. F_b, the black body flux in Eq (1.1), may be replaced by σT^4, giving the expression,

$$\epsilon_f(u) = F(u,T)/\sigma T^4 \qquad (1.2)$$

where "u" is the optical depth of the absorber. The increment of optical depth is given by: $du = \bar{q}\, dp/g$. In this case the energies are integrated over all directions within a hemisphere subtended at the element of surface. We have not specified that $\epsilon_f(u)$ is not also a

function of temperature. The presence or absence of this specification will not alter the following treatment. The flux arising from the IR emission and transmission in an isothermal atmosphere above or below any level we consider follows from Eq (1.2) and is given by:

$$F(u,T) = \epsilon_f(u)\,\sigma T^4 \tag{1.3}$$

Since we are concerned with flux emissivity as a function of optical depth for several atmospheric slabs, we differentiate Eq (1.3) with respect to, "u", the optical depth, giving:

$$dF(u,T)/du = \sigma T^4 (d\,\epsilon_f(u)/du) \tag{1.4}$$

To integrate Eq (1.4) with respect to optical depth, we consider an atmosphere with arbitrary vertical distribution of radiating materials. We further assume horizontal stratification, that is, "u", "T", and "ϵ_d" are independent of the horizontal co-ordinates and are functions of height alone. Integrating over thin layers of optical depth, each with an assumed constant temperature, we obtain for the upward or downward flux at a reference level, r, in the atmosphere:

$$F_r(u,T) = \int_0^u \sigma \bar{T}^4(u)\,(\partial \epsilon_f(u)/\partial u)\,du \tag{1.5}$$

In computing downward flux from an arbitrary level, we integrate upward to the top of the water vapor atmosphere. The direction of integration is downward to the earth's surface for the upward flux.

It is best for this work to consider the upward flux of radiation with a known black background and also a known optical depth (precipitable centimeters of atmospheric water vapor) from the earth's surface to the various levels of observation. The background for the downward flux would be difficult to ascertain.

2. Instrumentation

The radiometersonde (Suomi and Kuhn, 1958) is essentially a radiosonde, measuring temperature, pressure, and humidity in the usual way plus a radiometer directly measuring atmospheric, terrestrial, and solar energy illuminating its upper and lower surfaces. Fig. 1 illustrates the vertical components of the IR flux as they impinge on a radiometer in a plane parallel to the earth's surface. The accuracy of the radiometer has been discussed in the literature (Bushnell and Suomi, 1961; Kuhn, 1961). A review of the various tests and statements on its accuracy are contained in the Appendix.

The hygristor, upon which our moisture measurements depend, was developed by Dunmore (1938). It has a lag coefficient, for 1,000 feet per minute ventilation, ranging from 4 seconds at 25C to 120 seconds at -30C (Ference, 1951) and for a relative humidity of 90 percent. The hygristor can be adversely affected by polarization, washing effects of liquid water droplets on the element, insensitivity at high humidities, and variation in the shape of the humidity-resistance curve. Under average conditions (Middleton and Spilhaus, 1953) this electrolytic strip can measure relative humidity with a probable error of ± 2.5 percent at -10C and between 15 and 96 percent relative humidity. This probable error was ascertained for cloudy and clear conditions. Since we have made no measurements in the presence of clouds, the probable error to our measurements will be less. Assuming a probable error of ± 5.0 percent for a typical radiometersonde ascent of 9 January, 1961 at Oklahoma City, determined to be clear and cloudless, the numerical computation of the upward IR flux from the two relative humidities, one

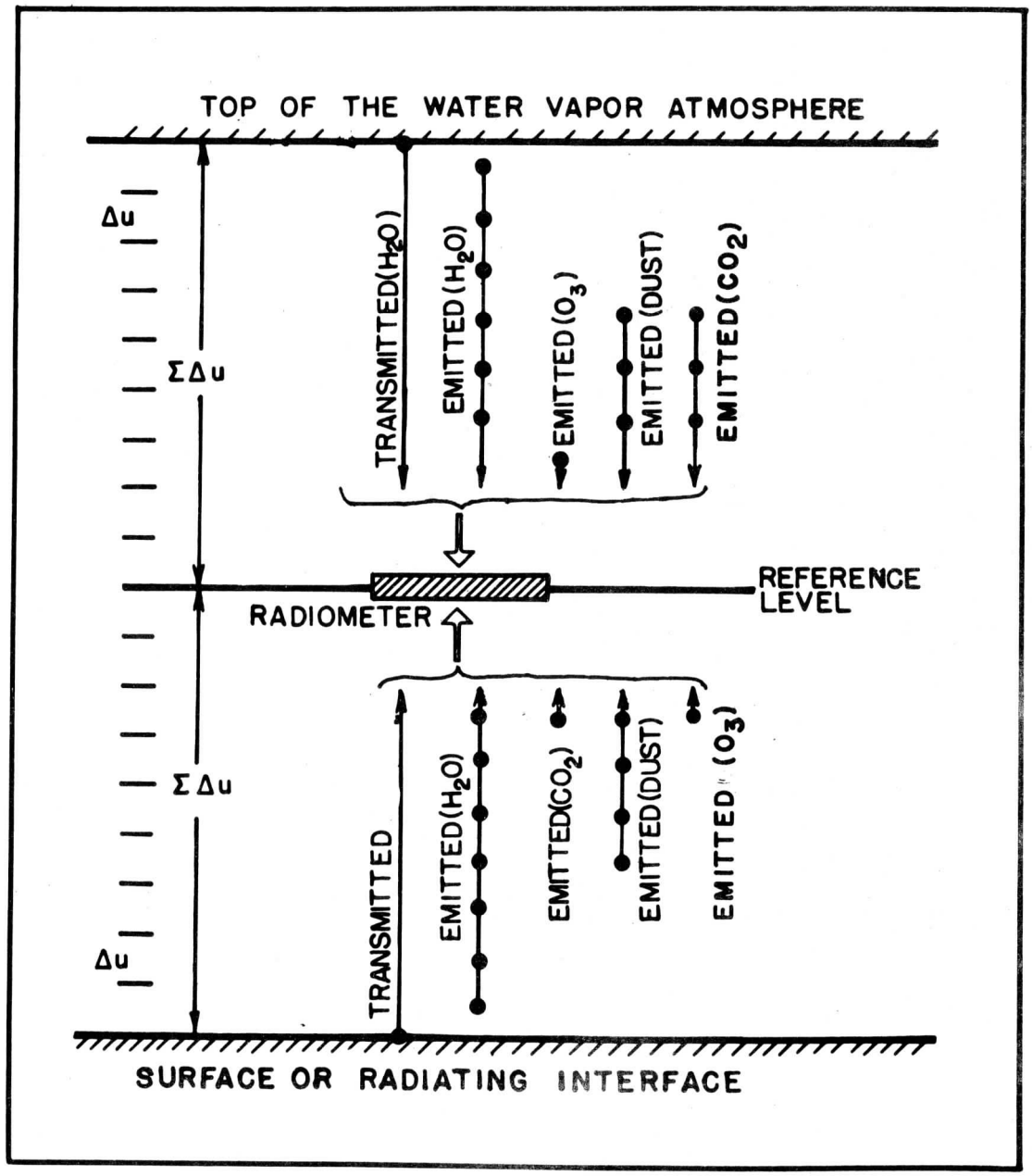
TOP OF THE WATER VAPOR ATMOSPHERE
Δu
ΣΔu
TRANSMITTED(H_2O)
EMITTED(H_2O)
EMITTED(O_3)
EMITTED(DUST)
EMITTED(CO_2)
REFERENCE LEVEL
RADIOMETER
ΣΔu
Δu
TRANSMITTED
EMITTED(H_2O)
EMITTED(CO_2)
EMITTED(DUST)
EMITTED (O_3)
SURFACE OR RADIATING INTERFACE

Figure 1

5 percent high and the other 5 percent low, gave an average difference for all levels of .007 cal cm^{-2} mm^{-1} (4.9 watts $meter^{-2}$). Since temperature and pressure enter into our measurements only as ratios, it is clear that our greatest chance for error lies in the humidity measurements with the hygristor. Fortunately, most of our humidity measuring is done within the region of best accuracy of the hygristor. Moreover, the amount of data provides statistical reliability.

An important radiometersonde ascent was made on the 28th of April in 1958 at Denver, Colorado. This flight was made simultaneously with an ascent of Dinger's (1961) frost point instrument and is cited here for that reason. A frost point instrument has the important advantage in that it possesses a constant percentage error over the entire range of atmospheric water vapor. In this particular ascent a height of 9 millibars was attained. The optical depth at these stratospheric heights, when measured downward from the highest reference level, was extremely shallow. Dinger indicated that his descent values of the measured frost point were reliable and thus we were able to place as much reliability into our computed mixing ratios and optical depths made from the frost points down to 67 millibars. Below 67 millibars the accuracy of the frost point instrument is questioned by Dinger. Unfortunately this prevented a low level comparison of the hygristor and frost point measured optical depths. During this high level measurement, no appreciable ozone was reported in simultaneous ozone instrument ascents. The probable maximum O_3 radiative contribution to the upward stream would be but .005 cal cm^{-2} mm^{-1} (3.5 watts $meter^{-2}$).

3. Determination of Water Vapor Flux Emissivity

Sky and Boundary Condition Criteria

Out of 300 radiometersonde ascents examined only 37 were suitable for flux emissivity measurements. No liquid water can be present in that portion of the ascent where such measurements are being made. Thus, the sky must be cloudless. A sound test for cloudless conditions is a plot of measured net radiation from a radiometersonde ascent on a log axis versus a linear plot of the optical depth (Brooks, 1941). Clear sky net radiation plots essentially as a straight line from minimum optical depths well out to long path lengths. On the other hand, net radiation through cloudy skies deviates sharply from this straight line plot. This is due to the high emissivity of liquid water or ice particles affecting both upward and downward IR flux, and consequently the net radiation. Cloudless sky ascents were selected in this manner after a prior check of the surface observation at the time of the ascent. Fig. 2a illustrates a plot for cloudless sky conditions, and for contrast, a reported cloudy ascent, Fig. 2b. The plot of net radiation clearly verifies the "cloudy" observation. Fig. 2c illustrates a reported "cloudless" ascent that was rejected. This test was applied to all ascents.

Since we are computing emissivity from direct measurements of the upward IR flux, we must know the air-interface radiative equilibrium temperature. We require a black background equilibrium temperature for calculation of the transmitted IR flux. This will be near the air-earth or air-earth cover interface and not necessarily at shelter level. A 1.5C error in the absolute interface temperature for an average ascent out of our group produces a 4 percent error in the emissivity at an

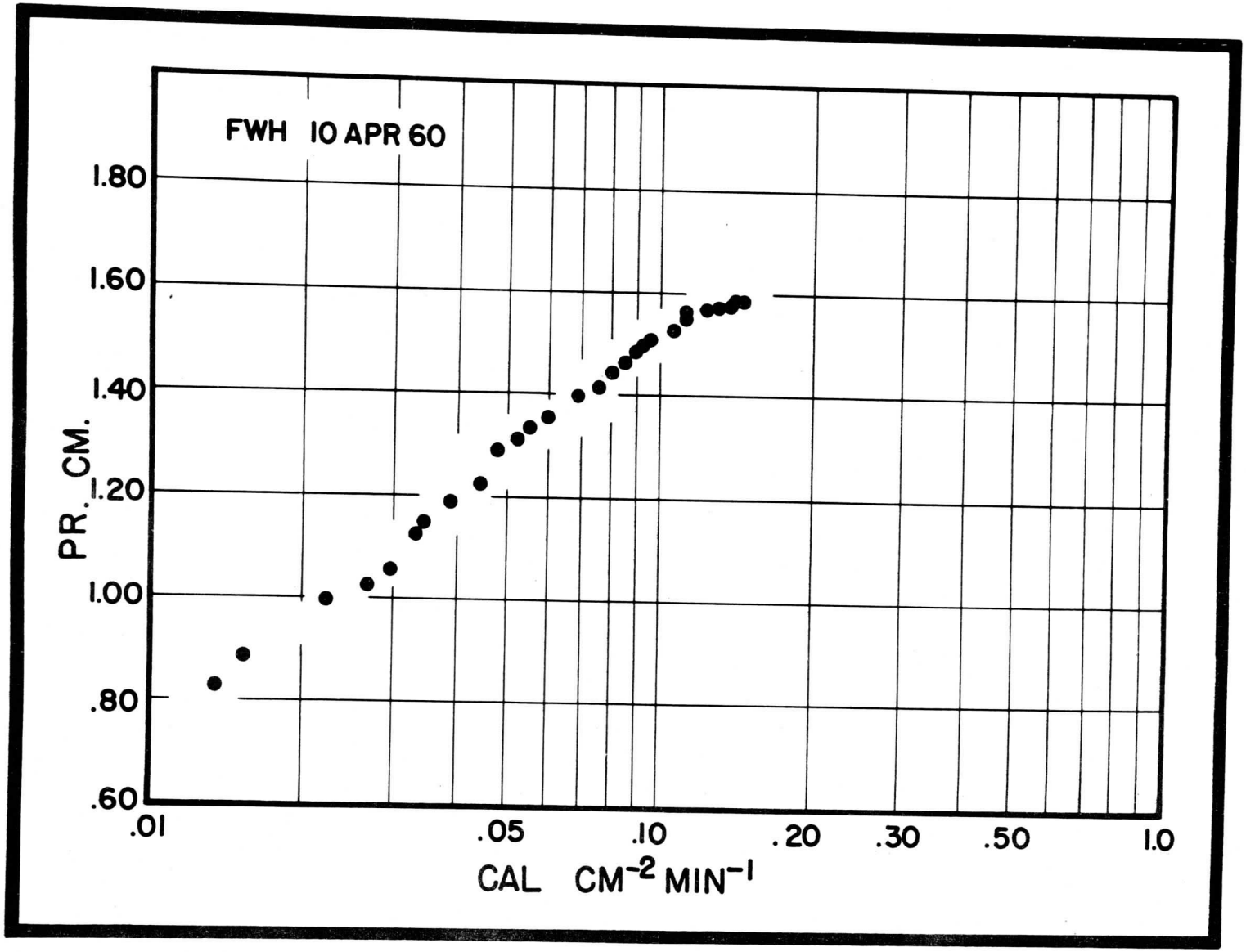
FWH 10 APR 60
1.80
1.60
1.40
1.20
1.00
.80
.60
PR. CM.
.01
.05
.10
.20
.30
.50
1.0
CAL CM-2 MIN-1

Figure 2a

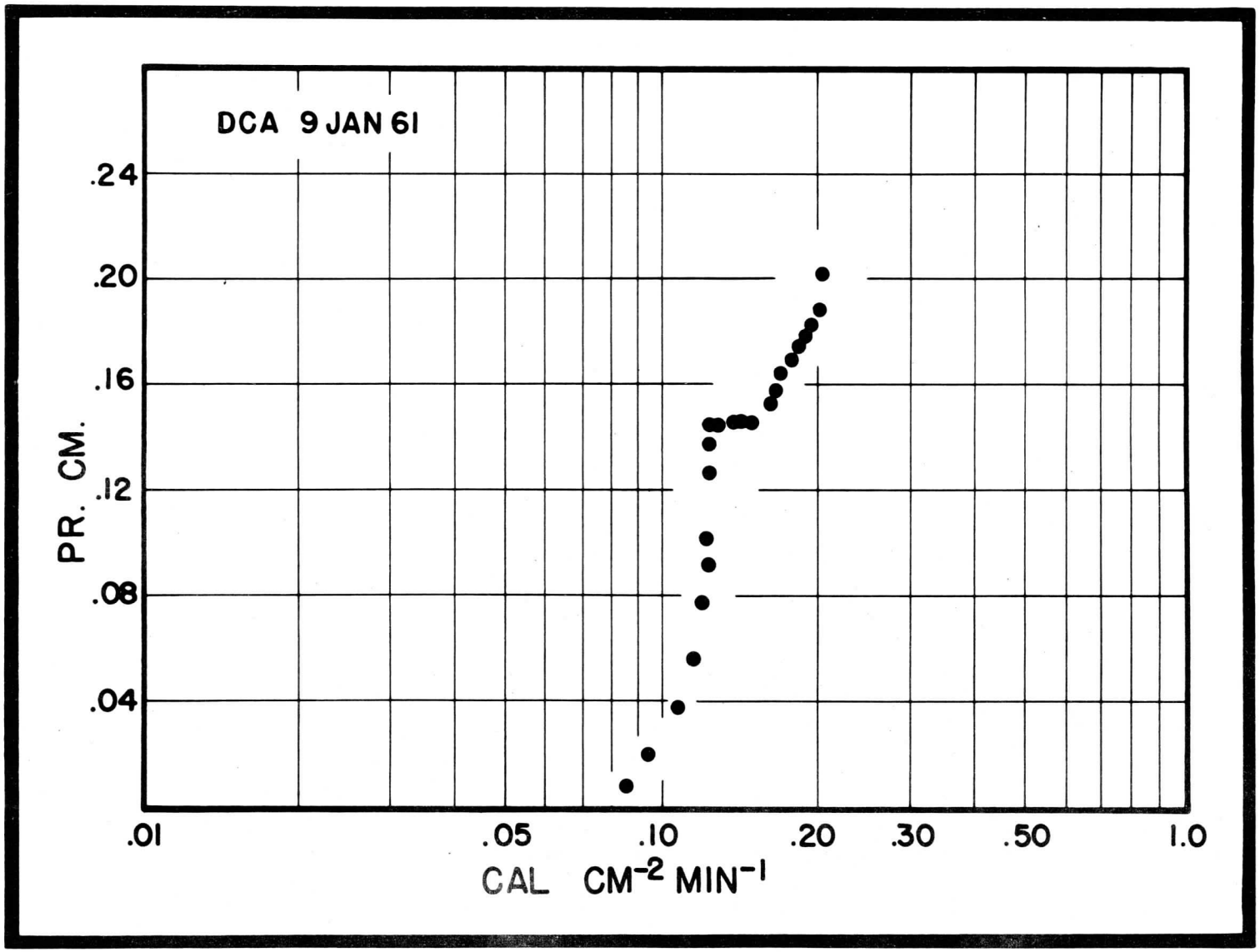

Figure 2c

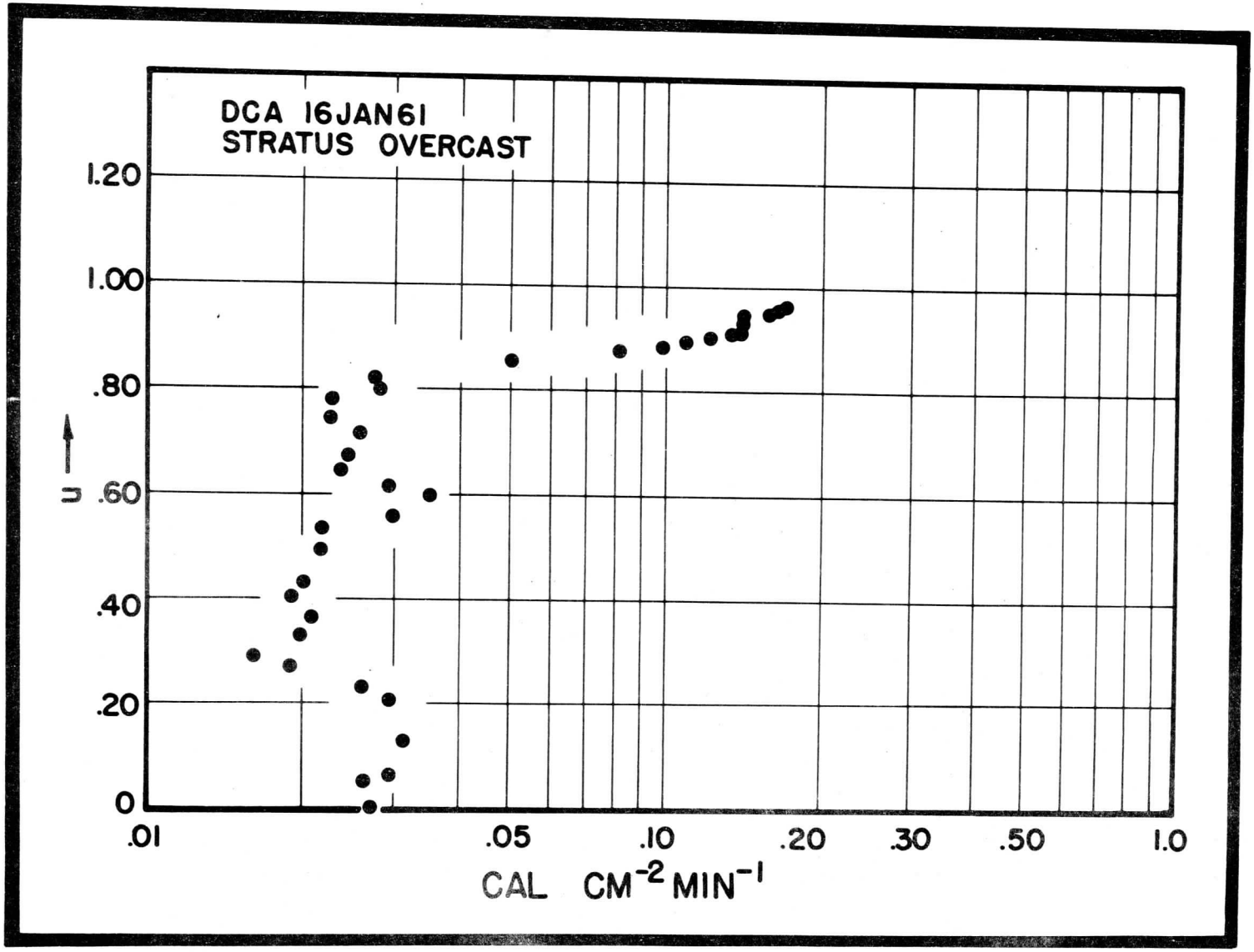
DCA 16JAN61
STRATUS OVERCAST
1.20
1.00
.80
.60
.40
.20
0
n
.01
.05
.10
.20
.30
.50
1.0
CAL CM^{-2} MIN^{-1}

Figure 2b

optical depth of .05 precipitable centimeters. It produces a ± 3 percent error in emissivity at .5 precipitable centimeters, and it results in a ± 2.5 percent error at 1.0 precipitable centimeters. See Eq (3.2).

Since we require an "interface" radiative equilibrium temperature and not the shelter temperature we must choose ascent times when the shelter-surface temperature difference is the smallest. Lettau and Davidson (1957) have shown that this difference is least from 1730 to 1830 hours local standard time. It is fortunate that this was the time of release of the radiometersondes.

To at least approach a homogeneous underlying surface for the radiometer to "look at", we chose ascents with a wind velocity equal to or exceeding 5 knots. Such wind velocities tend to increase low level mixing and provide a more representative interface temperature. To further limit surface horizontal inhomogeneity we chose flights over winter terrain and a few flights over the sea surface. The latter choice is highly desirable but few flights over the sea occurred during cloudless conditions.

Since we are making direct measurements of IR flux, pressure, temperature and humidity as a function of height, it is possible to obtain the "surface" radiative equilibrium, T_o, from the radiometersonde itself. This was not possible for the point of release at the surface since the radiometersondes were not allowed to reach equilibrium. However, Eq (3.2) developed subsequently in this section may be solved for T_o by working down from the first reporting level above the surface when the intervening water vapor is taken into account, and using the

TABLE I

COMPUTED FLUX EMISSIVITY

	U	Ascent Numbers											
in U	(pr.cm.)	26	25	24	27	28	29	10	4	20	8	9	5
-1.30	.05	.362		.309	.380		.330			.310	.310	.280	.375
-1.00	.10			.350	.382		.408	.335	.400	.400	.352	.343	.432
- .82	.15		.433	.380	.384		.432	.370	.445	.468	.383	.419	.469
- .70	.20		.422	.402		.399		.399	.475		.410	.490	.495
- .60	.25		.408	.420		.420		.420	.493		.425		
- .52	.30			.433		.438		.438	.502				
- .46	.35			.444		.452		.452					
- .40	.40			.451		.465		.465					
- .35	.45			.460		.472		.472					
- .30	.50			.462		.482		.482					.555
- .24	.55			.463		.488		.488					
- .22	.60			.464		.492		.492					
- .19	.65			.465		.500		.500					
- .155	.70					.505		.505					
- .125	.75												
- .10	.80												
- .07	.85												
- .046	.90												
- .023	.95												
0.0	1.00												
1.02	1.05												
1.04	1.10												

Table I

Computed Flux Emissivity continued

	U	Ascent Numbers														
in U	(pr.cm.)	13	14	15	16	17	18	30	1	11	22	23	6	31	32	33	34
-1.30	.05	.310	.280		.330		.310	.300	.349	.342							
-1.00	.10	.350	.368	.343	.372		.370	.360	.388	.380	.330	.410					
- .82	.15	.381	.415	.395	.400		.414	.410	.412	.408	.360	.440	.415				
- .70	.20	.406	.445	.435	.422	.375	.448	.463		.433	.392	.458	.434				
- .60	.25	.426		.466	.442	.400	.477			.450	.427	.470	.449				
- .52	.30	.441		.488	.460		.500			.463	.451	.483	.459				
- .46	.35	.456		.505	.473		.518			.474	.480	.500	.465				
- .40	.40	.467		.520	.484					.481	.490	.506	.473				
- .35	.45			.532	.497					.487	.491	.520					
- .30	.50			.545	.505					.490	.500	.528					
- .24	.55			.553	.515					.492	.508						
- .22	.60				.525						.512						
- .19	.65				.534						.516						
- .155	.70				.542						.516						
- .125	.75																
- .10	.80													.521	.529	.520	.528
- .07	.85																
- .046	.90													.530	.536	.530	.537
- .023	.95																
0.0	1.00													.538	.547	.537	.546
1.02	1.05																
1.04	1.10																

Table I

Computed Flux Emissivity continued

log U	U (pr.cm.)	Ascent Numbers 1	2	3	log U	U	36	37	38	39	40	41	42
-1.30	.05				-1.82	.015						.216	
-1.00	.10				-1.6	.025	.326	.260		.271	.306	.277	
- .82	.15	.367	.367	.	-1.46	.035		.323	.335	.288	.356	.348	
- .70	.20		.410		-1.35	.045	.334	.359	.352	.280	.306		
- .60	.25		.442		-1.26	.053	.419	.383	.325	.404			
- .52	.30		.468	.419	-1.19	.065		.393	.404	.400			
- .46	.35		.484	.445	-1.12	.075		.396	.374	.391			
- .40	.40		.475	.472	-1.07	.085		.402		.371			
- .35	.45		.481	.486		.095							
- .30	.50		.492	.500		.105							
- .24	.55		.496	.502		.115							
- .22	.60		.500	.503		.125							
- .19	.65					.0000550							.030
- .155	.70					.0000577							.031
- .125	.75												
- .10	.80												
- .07	.85												
- .046	.90												
- .023	.95												
0.0	1.00												
1.02	1.05												
1.04	1.10												

observed upward IR flux for $F_o\uparrow$. As an approximation, Robinson's (1950) water vapor emissivities were used. This was done for all ascents and the final temperature so computed was used if it did not depart from the shelter temperature by over $\pm$ 6.0C.

Flux Emissivity Computations

Eq (1.8) may be written in finite difference notation after adding carbon dioxide and ozone emission and transmission, giving:

$$F_r\uparrow = \sum_{i=1}^{2} \sigma T^4_{i-1/2}(u)_w \Delta\epsilon_i(u)_w + \sum_{i=1}^{n} \sigma T^4_{i-1/2}(u)_c \Delta\epsilon_i(u)_c + \sum_{i=1}^{n} \sigma T^4_{i-1/2}(u)_o \Delta\epsilon_i(u)_o + \left\{1.0 - \sum_{i=1}^{n} \Delta\epsilon_i(u)_w - \sum_{i=1}^{n} \Delta\epsilon_i(u)_c - \sum_{i=1}^{n} \Delta\epsilon_i(u)_o\right\} \sigma T_o^4 \quad (3.1)$$

In this equation the second and third terms on the right are the carbon dioxide and ozone emission, respectively. The last term is the atmospheric transmission term. This equation assumes a uniform distribution of carbon dioxide in percent by volume. It further assumes a knowledge of the quantity of ozone present in the atmosphere. We eliminated the ozone emission and transmission by choosing times and levels in the atmosphere with little or no ozone present.

The summations in Eq (3.1) are valid over relatively thin isothermal slabs. The typical lapse of temperature may be replaced by a series of isothermal slabs of differing mean temperature, indicated in Fig. 3. Eq (3.1) is used in evaluating the upward or downward IR flux for the generally, non-isothermal atmosphere. Eq (3.1) is re-written into a recursion formula which permits an explicit solution of the water vapor flux emissivity, omitting the ozone contribution.

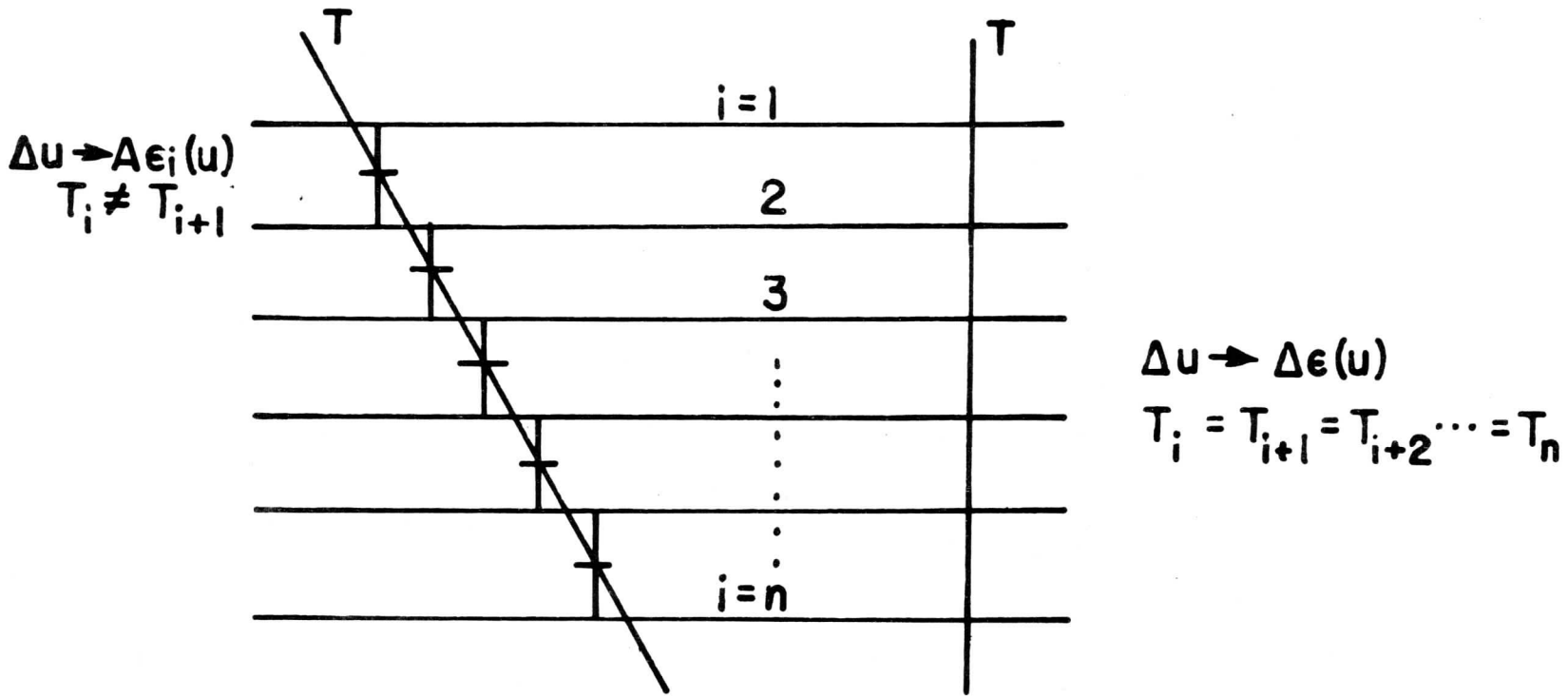

Figure 3

The resulting recursion equation is expressed by:

$$\epsilon_n(u)_w = \epsilon_{n-1}(u)_w + F_0\uparrow - \Sigma(\sigma T_{i-\frac{1}{2}}^4 - \sigma T_0^4)\Delta\epsilon_i(u)_w / \sigma T_{n-\frac{1}{2}}^4 - \sigma T_0^4 - \left\{\Sigma \sigma T_{i-\frac{1}{2}}^4 (u)_c \Delta\epsilon_i(u)_c + (1.0 - \Sigma\Delta\epsilon_i(u)_c)\sigma T_0^4 / \sigma T_{n-\frac{1}{2}}^4 - \sigma T_0^4\right\} \quad (3.2)$$

A solution of Eq (3.2) requires equal intervals of optical depth. This is so since each ϵ_f is a function of u and since each succeeding solution depends upon the preceding result. To meet this condition we transform the vertical axis from one of pressure to one of equal optical depth intervals, interpolating where necessary. An examination of the summations required in Eq (3.2) will readily show this to be necessary.

We smoothed the flux emissivity results for each flight by a simple two point overlapping mean. No non-linear terms were smoothed. This technique tended to eliminate not only noise in the radiometersonde measurement but also noise in the humidity measurements. Eq (3.2) was solved on a high speed digital computer.

4. Results and Theoretical Implications

Comparison of Flux Emissivity Results

In order to compare our results with those of other researchers, the flux emissivities were evaluated for a linear pressure reduced optical depth. They represent a computer solution of Eq (3.2). The emissivities are listed in Table I and are presented as an ensemble of data points in Fig. 4.

The table containing 211 points includes the two extremely shallow optical depths measured in the stratosphere. The scatter in our data points is quite similar to Fig. 4 of Robinson (1950), covering measure-

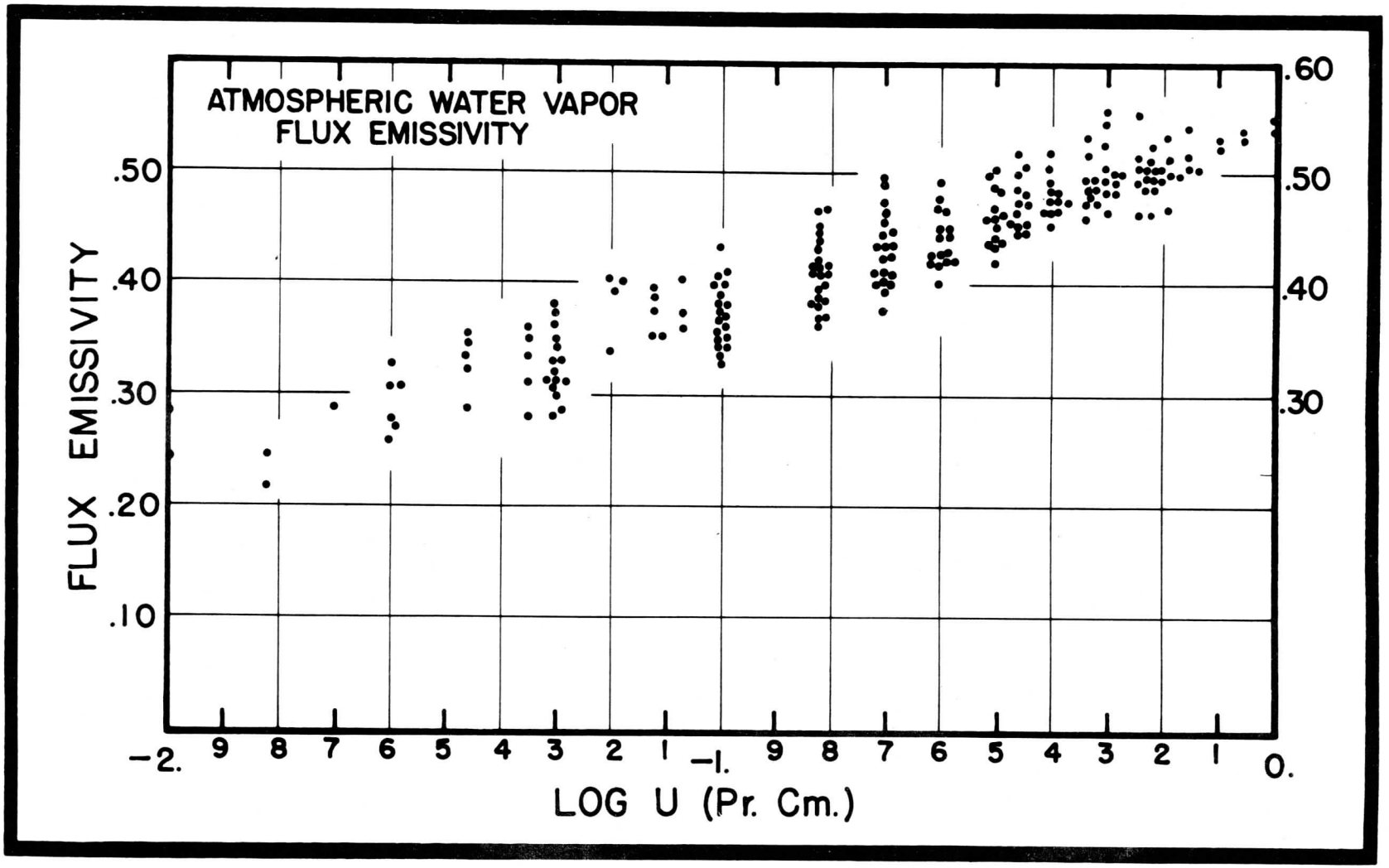
ATMOSPHERIC WATER VAPOR
FLUX EMISSIVITY
FLUX EMISSIVITY
.50
.40
.30
.20
.10
.60
.50
.40
.30
−2.
9
8
7
6
5
4
3
2
1
−1.
9
8
7
6
5
4
3
2
1
0.
LOG U (Pr. Cm.)

Figure 4

ments made at the surface. Robinson drew a smoothed curve to the lower envelope or minima of his plotted points. In comparing our data points, Fig. 4, with the curves of other researchers we obtained a curve of best fit to the data by least squares. We chose a model for a power series of the form:

$$\ln (1.0 - \epsilon_f) = \ln A - ku + a_2 u^2 + \ldots\ldots a_n u^n \qquad (4.1)$$

where ln A is equivalent to a_0 and -k to a_1. This physical model reflects an exponential decrease in the emissivity with decreasing optical depth. The quadratic and higher order terms are corrector terms. The measure for the polynomial of best fit was the unbiased standard error,

$$S.E. = \left\{ \left(\sum_{i=1}^{n} (y_i - \hat{y}_i)^2 \right) / N - \text{no. of coefficients} \right\}^{1/2} \qquad (4.2)$$

The method of fit was that of Gauss-Jordan by Griffith (1961). For this data, a fifth order polynomial gave the best fit on the basis of the least unbiased standard error. The final evaluated curve for the polynomial is given in Fig. 5, which also includes the curves of Elsasser (1960), Robinson (1950) and Bruinenberg (1946).

In spite of few data below .001 precipitable centimeters other than the important stratospheric values at .0000577 precipitable centimeters and at .00005 precipitable centimeters we agree very well with the laboratory values of Howard, Burch and Williams (1955) used by Elsasser (1960), and re-computed as flux emissivities. Elsasser's curves were generated from a computer program of Bushnell (1961), where flux emissivity is given by:

$$\epsilon_f(u)_w = \left\{ \sum_{i=1}^{n} F_\lambda(T) \left(1.0 - \tau(u L(u))\right) \right\} / \sigma T^4 \qquad (4.3)$$

Here L(u) is Elsasser's generalized absorption coefficient (1960). The

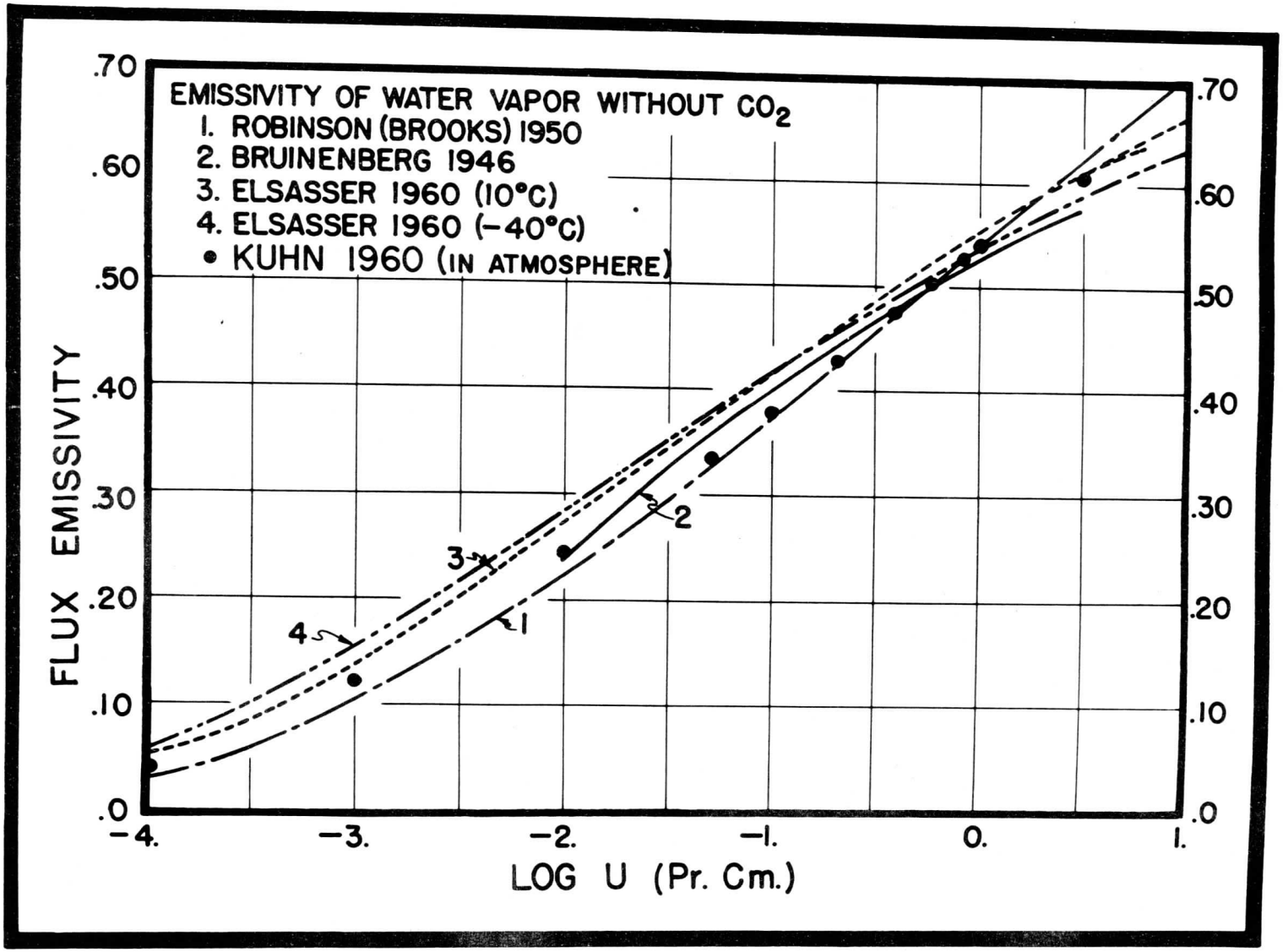
EMISSIVITY OF WATER VAPOR WITHOUT CO_2
1. ROBINSON (BROOKS) 1950
2. BRUINENBERG 1946
3. ELSASSER 1960 (10°C)
4. ELSASSER 1960 (−40°C)
• KUHN 1960 (IN ATMOSPHERE)
FLUX EMISSIVITY
.70
.60
.50
.40
.30
.20
.10
.0
−4.
−3.
−2.
−1.
0.
1.
LOG U (Pr. Cm.)
1
2
3
4

Figure 5

agreement between curves is well within experimental error and our "in situ" measurements lend support to the various adopted slab emissivities. This agreement is better with Robinson's (1950) curves than with Elsasser's (1960) curves.

Temperature Dependence of Flux Emissivity

Temperature affects water vapor flux emissivity in two ways. First, it shifts the black body (Planckian) energy distribution as a function of wavelength to wavelengths of strong H_2O vapor absorption or emission. Secondly, it changes the intensity of the absorption or emission band. The first effect produces a reduction in emission with increasing temperature due to the progressive shift of the peak of the black body energy distribution away from the intense rotational absorption band of the H_2O vapor spectrum towards the transparent region around 10μ. As a result of this shift, alone, the absorptivity at 20C would be from 15 to 35 percent less than at -40C, the greater variation occurring with smaller path lengths of precipitable water (Deacon, 1950). The second effect, the increasing intensity of the absorption bands, mainly in the wings of the bands, with rising temperature works in opposition to the first effect. Experimental evidence is meager on this point. It was not felt that our experiment was sensitive enough to detect changes in such small effects, consequently we have used $(T_o)^{.5}$ as the temperature corrector to the optical depth.

Pressure Dependence of Flux Emissivity

The far IR bands which cause radiative transfer in the atmosphere consist of numerous spectral lines. Considering one of these spectral

lines and designating the integrated intensity of the line by "S", the distribution of absorption along the Lorentz line shape is given by:

$$k_\lambda = S\alpha/\pi\left(1/\lambda - 1/\lambda_0\right)^2 + \alpha^2 \qquad (4.4)$$

where α is defined as the half-width of the line. According to Lorentz (1905) α is proportional to molecular collision frequency and is thus directly proportional to density times mean velocity. Mean velocity is proportional to the square root of the temperature. The half-width, then, is directly proportional to the pressure and inversely proportional to the square root of the temperature, giving

$$\alpha = \left\{\alpha_0\, p\,(T_0/T)^{1/2}\right\}/p_0 \qquad (4.5)$$

The pressure broadening effect, of course, is different for the various absorbers.

The total absorption of a spectral line $A_\lambda d_\lambda$ over a spectral interval after Ladenburg and Reiche (1913) and more recently, Howard, Burch and Williams (1955), is given by:

$$\int_0^\infty A_\lambda d_\lambda = 2\pi\alpha x e^{-x}\left\{I_0(ix) - iI_1(ix)\right\} = 2\pi\alpha f(x), \qquad (4.6)$$

Where $x = Su/2\pi\alpha$.

Here they (Howard, Burch, and Williams) point out that where $x = Su/2\pi\alpha$. It is interesting to study the behavior of Eq (4.6) for large and for small x. These are two limiting cases and yield two different solutions for the total absorption. For small x, weak lines or thin absorber, from Eq (4.6) it can be shown that,

$$\int_0^\infty A_\lambda d_\lambda = 2\pi\alpha x = Su \qquad (4.7)$$

Here the total absorption is equal to the product of the line intensity, S, and the layer thickness, u, and is independent of pressure. In this case, only the center of the line is important. On the other hand,

in the actual atmosphere, we are in a position to investigate the effects where limits are given in Eqs (4.7) and (4.8), not over a single spectral line, but over a good portion of the IR spectrum.

We require a value for the exponent of the pressure reduction ratio, γ, which provides a curve of best fit for all the measured emissivity data against optical depth, and which minimizes errors arising from fluctuations of emissivities about its mean, at discrete optical depths. We have defined the reduced optical depth, u^*, in Eq (4.9), where γ is the power of the pressure ratio. Kaplan (1952), Elsasser (1960) and others have stated that γ should be 1., at least for a single spectral line. Brooks (1950) and Bruinenberg (1946) have computed the effective optical depth for their radiation charts with $\gamma = .5$. Studies by Manabe and Moller (1962) and others for band spectra rather than line spectra indicate a less than linear value for γ.

To obtain a best fit to previously computed emissivities we can vary γ in Eq (4.9) and look for a resulting minimum in the unbiased standard error defined by Eq (4.2). Since the atmosphere is a combination of strong and weak spectral lines and deep and shallow optical depths, we felt γ would be less than 1.0. A linear pressure reduction to the optical depth as called for in the theory of a single spectral line might not hold for a band or for a very thin gas. Consequently, we stepped γ from 1.1 down to .5 and fitted new curves to the data. The resulting standard errors for each curve are plotted in Fig. 6a. Evidently, a pressure reduction of the form $(p/p_o)^\gamma$ where $\gamma = .85$, minimized deviations of our data points from the fitted curve.

for large x, strong lines and thick absorber, the solution obtains:

$$\int_0^\infty \bar{A}_\lambda d\lambda = 2\sqrt{S\alpha(p)u} \qquad (4.8)$$

Here the wings are also important and are strongly affected by pressure broadening. Theory for a single line shows that pressure broadening appears as a linear term under the radical in Eq (4.8). This has been verified by Townes and Merritt (1946). To take into account pressure broadening on the half width α, as in Eq (4.5) we note the product "$\alpha(p)u$" in Eq (4.8) and introduce in Eq (4.8) the pressure reduced optical depth expressed by:

$$u^* = u\,(p/p_0)^\gamma, \text{ where } \gamma = 1 \qquad (4.9)$$

where γ is equal to 1. This gives for the total absorption:

$$\int_0^\infty \bar{A}_\lambda d\lambda = 2\sqrt{S\alpha\,(p/p_0)(T_0/T)^{.5}u} \qquad (4.10)$$

and the single line linear pressure reduction to optical depth is evident.

Atmospheric water vapor displays absorption bands that are a mixture of strong lines and weak lines. When the line intensity is weak or the absorbing water vapor is very thin, (small x in Eq (4.6)) the total absorption is proportional to the product of line intensity and the amount of water vapor (Manabe and Moller, 1962). In this case it is independent of pressure and γ may well approach or be less than the half power. Kaplan (1954) and Manabe and Moller (1962) both indicate that linear scaling tends to overestimate the pressure effect for moderately weak lines and, we may add, for very thin absorbers.

Since we have measurements of emissivity (absorptivity) under a wide range of conditions of pressure, temperature and optical depth,

However, a "plateau" appears at $\gamma = .7$. We can conclude that $\gamma = .85$, which is "slower" than a linear reduction, provides the best fit of emissivity versus optical depth for all our data. Some of the emissivities obtained at shorter path lengths and lower pressures indicates that γ equal to .85 is still too strong.

The tendency toward a square root or at least a lesser reduction than $(p/p_s)^{.85}$ unfortunately cannot be checked further until we have more measurements at shorter path lengths such as the two measurements made in the stratosphere. It may not be possible to obtain a single value for γ. Others have also proposed this idea. This would lead to a γ (p) relationship which would not over-reduce at low pressures and shallow optical depths, and yet which would function throughout the atmosphere.

An examination of the data points of Fig. 4 revealed that some twenty points, for log u equal to -1.9 up through log u equal to -0.2 were at lower than average pressure than the mean pressure of the data points at the various depths. By lower than average pressures we mean the lowest pressures for the particular optical depth. When these twenty cases were eliminated a new fit to the data provides a new plot of the standard errors for each fit (Fig. 6b).

We can conclude from Fig. 6 that the elimination of emissivity data points evaluated at low pressures results in a widening of the plot of the minimum standard errors and a removal of the plateau at $\gamma = .7$ in Fig. 6a. These primarily low to mid-tropospheric data points give evidence that a γ of .80 would give the most representative

pressure reduction. Of course, this last sample is biased toward deeper optical depths. An attempt was then made to express γ as a $\gamma(p)$. Moller (1944) suggested a pressure reduction to the optical depth of the form:

$$u^* = u\left\{.985\left(\bar{p}/p_o\right)^{.80} + .015\left(p_o/\bar{p}\right)\right\} \tag{4.11}$$

This "slows-up" the pressure reduction at low pressures, but becomes too large at low pressures. Using this as a guide we applied our "in situ" measurements to a further analysis of the pressure reduction. We used the relationship:

$$u^* = u\left\{\left(\bar{p}/p_o\right)^{.85} + .03\left(p_o/\bar{p}\right)\right\} \tag{4.12}$$

through 100 millibars. Above 100 millibars we used the relationship:

$$u^* = u\left\{-.00558\,\bar{p} + 1.00\right\} \tag{4.12}$$

These expressions for the pressure reduction gave essentially the same results as Eq (4.9) with $\gamma = .85$. This would be expected since we had few data at pressures lower than 400 millibars. Thus, the corrector $.03(p_o/p)$ in Eq (4.12a) and Eq (4.12b) would not have much effect on our data taken at tropospheric pressures. Consequently, we chose Eq (4.9) as the final expression.

Adopted Emissivities for Isothermal Atmospheric Slabs without Carbon Dioxide

Using $\gamma = .85$ in Eq (4.9) on the evidence of Fig. 6 a curve of best fit was secured to the data points of Fig. 4 between .05 and 1.0 precipitable centimeters. The change of the pressure reduction

exponent from 1.0 used in Fig. 4 to .85 for the new fit shifted the emissivity data points along the log u axis and reduced two standard errors to .038. The results appear in Fig. 7. Table 2 is a listing of the final emissivities at selected optical depths. We have no measured emissivity data points below log u of -2.0 until we reach those at log u equal to -4.25 and -4.25. A curve joining these points was drawn through a least squares interpolated value at log u of -3.0. Beyond log u of 0.0 a least squares interpolation extended the emissivity curve to log u equal to 0.5.

It was not possible to get many reliable experimental results above 1.0 precipitable centimeters. At such optical depths it was evident that cloud or particulate matter was present. To obtain a background radiating temperature for a rather nebulous cloud top was too ambiguous. By successive choices of the radiating surface temperature it was possible to secure values of emissivity which fitted the curve of Fig. 7 above 1.0 precipitable centimeters. However, this resulted in values that appeared to be well off the curve at optical depths below 1.0 precipitable centimeters (log u = 0.). The last point circled at log u of 0.5 is a machine interpolated value.

We used thirty-seven radiometersonde ascents in the atmosphere to determine water vapor flux emissivity curve. By extrapolation between .01 precipitable centimeters and .0001 precipitable centimeters we were able to extend the emissivity table over five decades of the logarithm of optical depth. The results are most reliable for optical depths typical of the troposphere. However, we were able to secure two

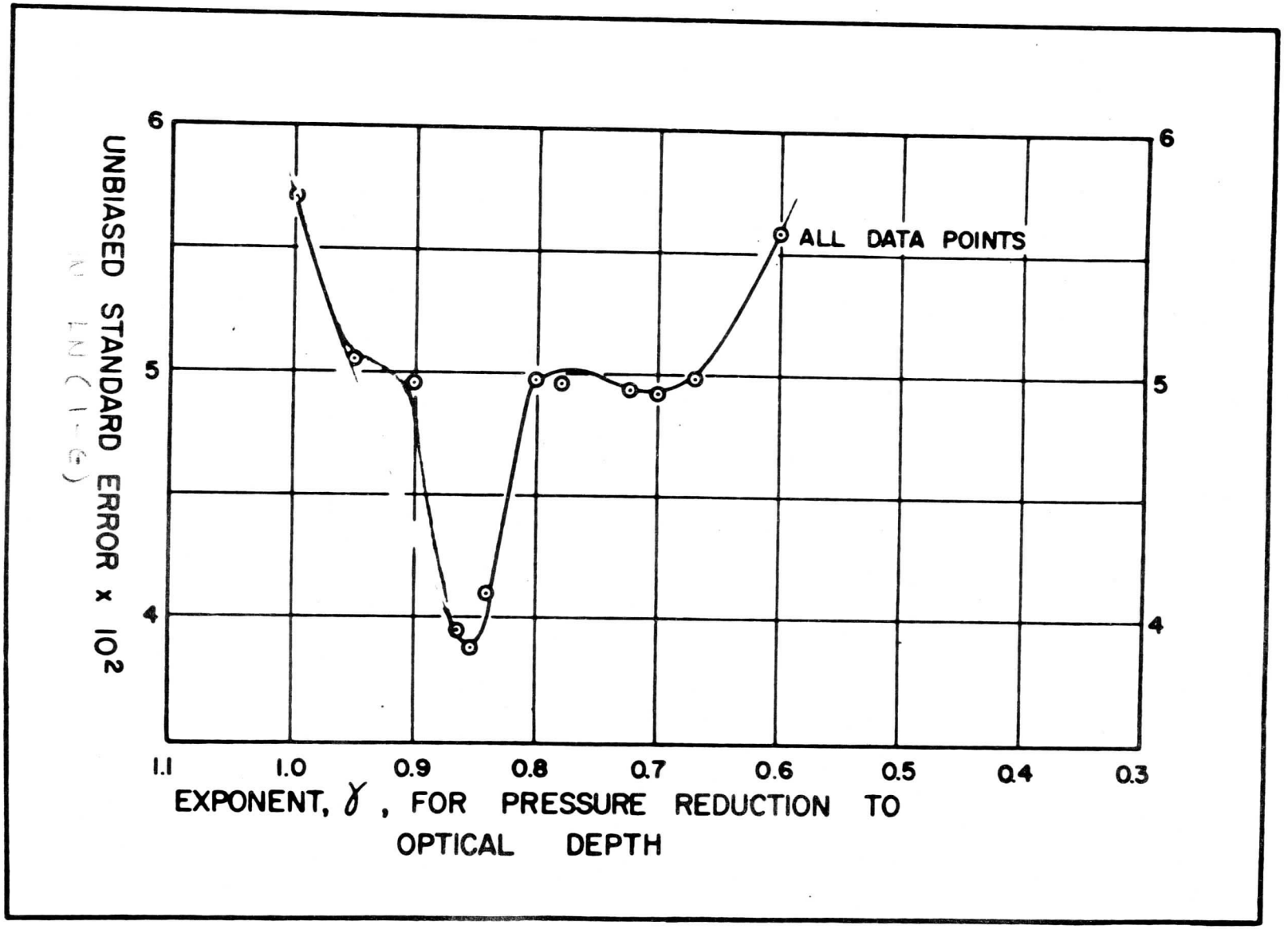
UNBIASED STANDARD ERROR x 10²
6
5
4
ALL DATA POINTS
1.1
1.0
0.9
0.8
0.7
0.6
0.5
0.4
0.3
EXPONENT, γ , FOR PRESSURE REDUCTION TO OPTICAL DEPTH

Figure 6a

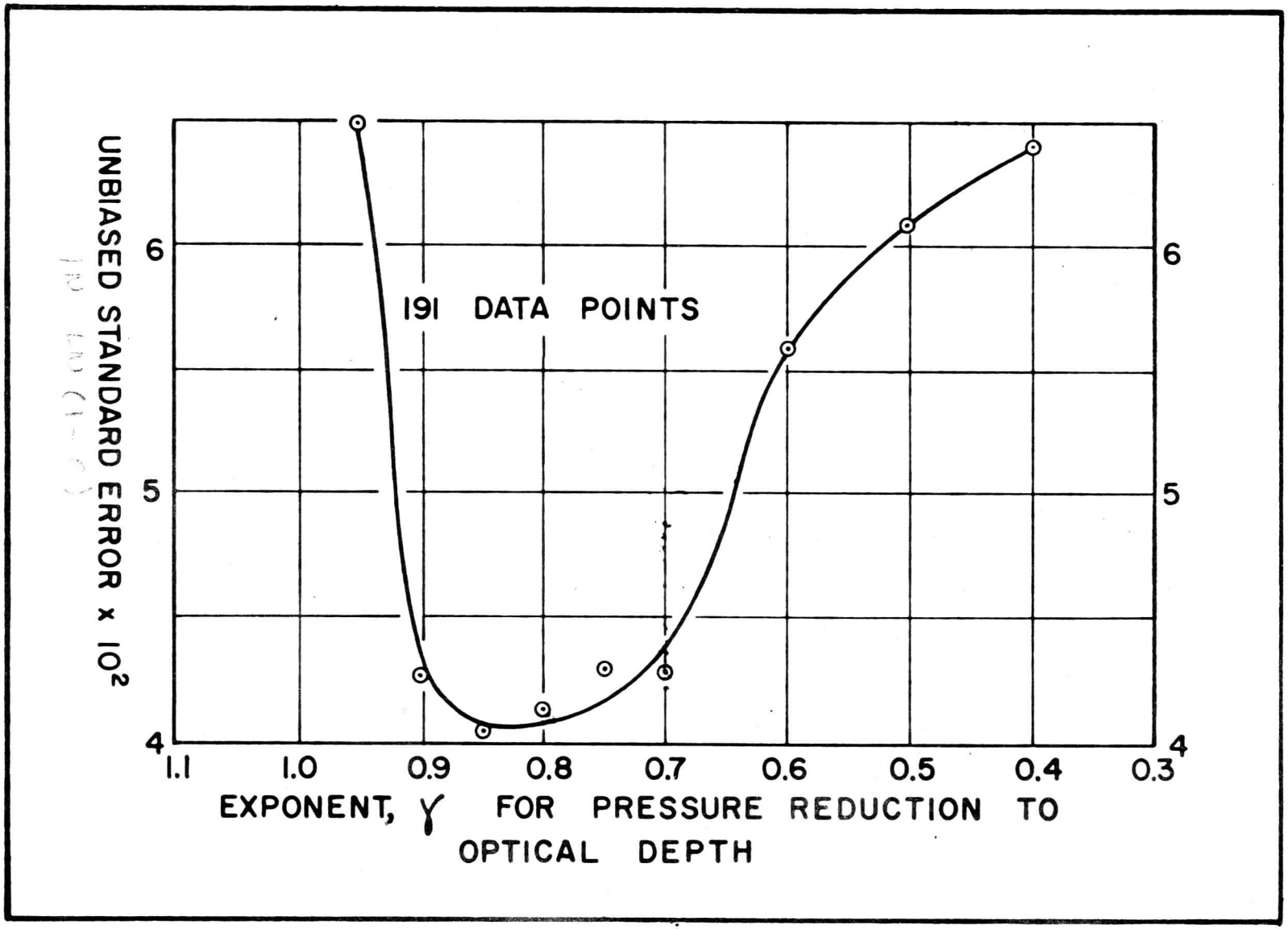
UNBIASED STANDARD ERROR x 10^2
6
5
4
191 DATA POINTS
1.1
1.0
0.9
0.8
0.7
0.6
0.5
0.4
0.3
EXPONENT, γ FOR PRESSURE REDUCTION TO OPTICAL DEPTH

Figure 6b

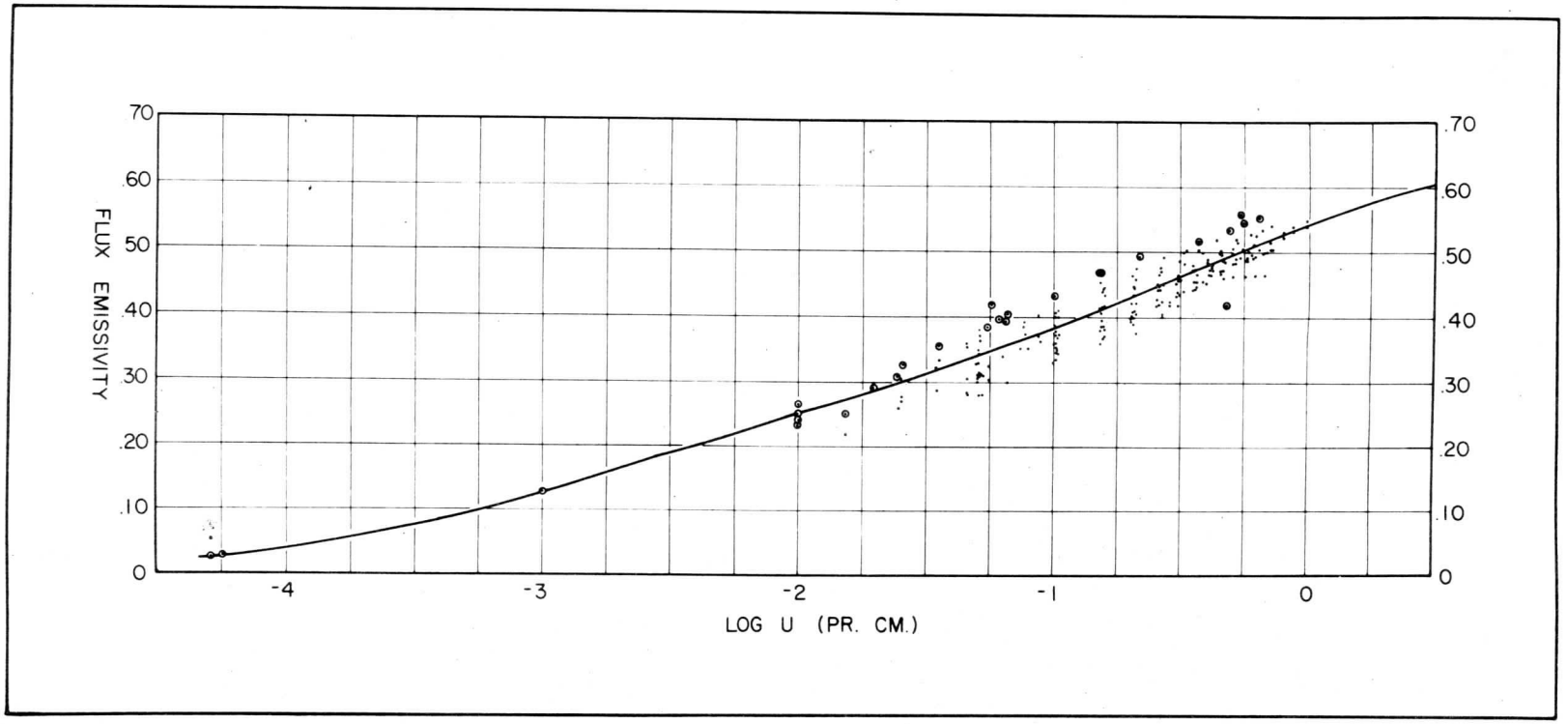
70
60
50
40
30
20
10
0
FLUX EMISSIVITY
.70
.60
.50
.40
.30
.20
.10
0
-4
-3
-2
-1
0
LOG U (PR. CM.)

Figure 7

reliable measurements in the stratosphere using frost point measurements to obtain emissivities at very shallow optical depths. In general, our slab emissivities for water vapor lie well within the range of previously used emissivities at least from .01 to 1.0 precipitable centimeters of water vapor.

In the course of the study we found observational evidence that a single pressure reduced optical depth will not serve for this wide range of optical depths. No further work can be profitable at very shallow optical depths until more atmospheric ascents of this nature can be made with frost point equipment or other suitable moisture measuring devices. On the other hand, radiosondes flights in cloudless tropical air can allow future work to extend these measurements one more decade toward deeper optical layers.

Table 2

Water Vapor Flux Emissivity as a function of Optical Depth without Carbon Dioxide

u (pr.cm.)	Emissivity(Water Vapor)
.0001	.040
.001	.128
.01	.249
.05	.339
.10	.381
.20	.430
.30	.459
.40	.478
.50	.495
.60	.508
.70	.517
.80	.526
.90	.534
1.00	.542
2.00	.586
3.00	.607

APPENDIX

Accuracy of the Radiometersonde

The basic expression for the evaluation of the measured upward IR flux by the radiometersonde is given (Suomi, Staley, Kuhn, 1958) by:

$$F_o\uparrow = \sigma T_b^4 + (1/a(1-aL))(k_i(T_b-T_t)/\Delta z_i - k_b(T_b-T_a)/\Delta z_b + \lambda(dT_b/dt)) \quad \text{(A1)}$$

The variables in Eq A1 are $F_o\uparrow$, T_b, k_1, T_t, k_b, T_a, and dt_b/dt. All other terms or symbols are constants whose values are given in the "List of Symbols." Any errors in $F_o\uparrow$ will be reflected as an error in the measurement of the flux emissivity. The accuracy of the flux emissivity measurements made from the observations of $F_o\uparrow$, temperature and humidity will be discussed at the conclusion of the Appendix. We divide the discussion on the accuracy of the radiometersonde into investigations of its static physical design and its operation in the atmospheric environment.

Initially, we consider errors in the measured flux due to possible incorrect polyethylene transmissivity measurements, or to an incorrect assumption of "flatness" in the transmissivity spectrum of polyethylene (Suomi and Kuhn, 1958). The error in this first instance, assumed to be two r.m.s. deviations ($2\sigma'$), and derived from Eq A1, is given by:

$$d F_o\uparrow = ((a^2(a-a^2L)^{-2})(k_i(T_b-T_t)/\Delta z_i - k_b(T_b-T_a)/\Delta z_b + \lambda(dT_b/dt)))(dL) \quad \text{(A2)}$$

Assuming a .03 error in the polyethylene transmissivity measurement, including departures from flatness; a normal mid-tropospheric conduction and lag transfer of .150 cal/cm^2 min (second term on right hand side of Eq A2); and a black surface absorptivity of .85, $2\sigma'$ equals .0051 cal/cm^2 min (3.6 watts/meter^2). In another experiment, Bushnell (1962) found $2\sigma'$ equal to 4.0 watts/meter^2 for two r.m.s.

deviations for the polyethylene.

In the case of the black sensing surfaces of the radiometer, possible errors in the measured diffuse absorpitvity of the black paint, inaccurate assumptions of its "flatness" (Suomi and Kuhn, 1958), or variability in the paint and spraying techniques can all contribute to an error in the employed absorptivity of the sensors. The error in $F_o\uparrow$ due to these questions can be expressed from Eq A1:

$$dF_o\uparrow = -((a-a^2L)^{-2}(1-2aL)\ (\text{conductivity} + \text{lag})\, dz) \qquad (A3)$$

The second term on the right in Eq A3 is identical to that in Eq A2. Assuming a .05 error in the black paint absorptivity; a polyethylene transmissivity of .18; and a conduction plus lag term of .15, $2\sigma'$ equals .006 cal/ cm^2 min (4.2 watts/meter^2). Bushnell (1962) found 3.0 watts/meter^2.

Considering possible errors in the conductivity of the internal section of the radiometer due to manufacturing variances in the combined air and expended polystyrene cells (1.25 lb/ft^3 density) the error express for $F_o\uparrow$ from Eq A1 is:

$$dF_o\uparrow = (1/a(1-aL))\,(dT/dz)\,d\,k_i \qquad (A4)$$

Assuming an error of .0005 cal/ C Cm min in the internal thermal conductivity; a 20C temperature gradient across the interior radiometer section and a vlue of 1.45 for the term, 1.0/(a(1.0-aL)), $2\sigma'$ equals .005 cal/ cm^2 min (3.5 watts/ meter^2). Bushnell (1962) found $2\sigma'$ equal to 1.0 watts/ meter^2.

A fabrication tolerance in the vertical dimension of the bottom air

cell and in the interior section of the radiometer of two millimeters in each results in $2\sigma'$ equal to .0045 cal/ cm^2 min (3.10 watts/meter^2) from Eq A1 by the expression:

$$dF_0\uparrow = -\left(\tfrac{1}{a}(1-aL)\right)\left(\left(k_i(T_b-T_t)\Delta z_i^{-2}dz_i + k_b(T_b-T_a)\Delta z_b^{-2}d\Delta z_b\right) \quad (A5)$$

For this result we have assumed a 20C gradient from the upper to the lower sensing surface of the radiometer and 10C from the outer polyethylene windshield to the bottom sensor. Bushnell found 1.8 watts/ meter^2 for $2\sigma'$.

The last physical design error to consider here will be the effects of a 0.5C error in the measured thermistor temperatures for a normal ascent under mid-tropospheric conditions. The error for this from Eq A1 is:

$$dF_0\uparrow = 4\sigma T_b^{\,3}\,dT_b \quad (A6)$$

Letting $1/a(1-aL) = 1.45$; $T_b = -15.0$C and $dt_b = dT_t = dT_a = 0.3$C, $2\sigma'$ equals .0030 cal/ cm^2 min (2.1 watts/ meter^2). Here, Bushnell (1962) found 1.1 watts/ meter^2.

Turning to errors in the radiometer under tropospheric operating conditions, the correct operation of the radiometer requires sufficient ventilation to effect an equality of ambient and upper and lower polyethylene temperatures. It is possible that at high altitudes sufficient ventilation may not occur. To check this effect, one radiometer heated from above by shielding and one standard unit were flown on the same balloon. The effect of shielding the upper surface on one unit was to increase the lower sensor temperature and approximately double the temperature gradient between the lower sensing surface and the lower poly-

ethylene shield. If ventilation decreased with height there should be a large discrepency in the measurement of the upward IR flux with the two radiometers. The shielded unit should give a substantially lower upward flux than that measured with the standard unit due to a possible conduction error caused by an assumption of equality between air and lower polyethylene temperatures. This did not occur. The mean difference during this flight for all measurements through 160 mb, F_o(unshielded) minus F_o(shielded), was .002 cal/cm^2 min (1.4 watts/meter^2) with an r.m.s. deviation of .006 cal/cm^2 min (4.2 watts/meter^2). Ventilation of the lower polyethylene surface does not appear to be a serious problem, at least in the troposphere.

The interception of radiation from the expanded "black" balloon, while it cannot bother the upward IR flux and resulting slab emissivity evaluation, can affect the downward IR flux. Assuming the balloon (600 gram Weather Bureau Sounding Type) is "black" at -10C and intercepts 1 percent of the total solid angle of $2\sigma'$ steradians, it would contribute at most .0034 cal/cm^2 min (2.8 watts/meter^2) to the downward stream of IR radiation and nothing to the upward.

The r.m.s. deviation in F_o obtained by summing the variances of all the possible errors discussed and extracting the square root is .0054 cal/cm^2 min. $2\sigma'$ is equal, then, to .0108 cal/cm^2 min (7.5 watts/meter^2). These results are summarized in Table A1. One r.m.s. deviation of .009 cal/cm^2 min, equal to the average of Bushnell's and our analysis, would cause an error of .070 in the measured emissivity at an optical depth of 0.5 precipitable centimeters, .03 larger than the observed r.m.s. deviation in Fig. 7 for our actual data. However, even though the error analysis has been made purposefully severe, it helps to explain the scatter of our emissivity results in Fig. 7.

Table A1

Error Analysis of F_0

Error Source	Derived from assumed maximum error: 2σ cal/cm^2 min	2σ watts/meter^2	Variance cal^2/cm^{4}min^2	Bushnell (1962): 2σ watts/meter^2	Variance cal^2/cm^{4}min^2
Polyethylene	.0051	3.6	6.5×10^{-6}	4.0	8.1×10^{-6}
Absorptivity paint	.0060	4.2	9.0×10^{-6}	3.0	4.6×10^{-6}
Internal Conduction	.0050	3.5	6.3×10^{-6}	1.0	0.5×10^{-6}
Vertical Dimensions	.0045	3.1	5.1×10^{-6}	1.8	1.7×10^{-6}
Temperature	.0030	2.1	2.3×10^{-6}	1.1	0.5×10^{-6}
Sum of Variance			29.2×10^{-6}		15.4×10^{-6}
r.m.s. deviation (σ)			.0054 ly/min		.0039 ly/min
2σ			.0108 ly/min		.0078 ly/min

REFERENCES

Brooks, D.L., 1950: A tabular method for the computation of temperature change by infrared radiation in the free atmosphere. J. Meteor., 7, 313-321.

Brooks, F. A., 1941: Observations of atmospheric radiation. Pap. phys. Ocean Meteor., Mass. Inst. Tech. and Woods Hole ocean. Instn., 8, No. 2, 23pp.

Bruinenberg, A., 1946: A numerical method for the calculation of temperature changes by radiation in the free atmosphere. (in Dutch). Kon. Nederl. Meteor. Inst., Meded, en Verhand, Serie B, Deel y, No. 1, 57 pp.

Bushnell, R. H., 1961: Personal communication with the author.

Bushnell, R. H., and V. E. Suomi, 1961: Experimental flight verification of the economical net radiometer. J. geophys. Res. 66, 2843-2848.

Bushnell, R. H., 1962: Personal communication with the author.

Deacon, E. L., 1950: Radioactive heat transfer in the air near the ground. Austr. J. Sci. Res., Ser. A., 3, 274-383.

Dinger, J. E., 1961: Personal communication with the author.

Dunmore, F. W., 1938: An electric hygrometer and its application to radio meteorography. (Res. Paper 1102), J. Res. Nat. Bur. Stand., 20, 723-744.

Elsasser, W. M., 1960: Atmospheric radiation tables., Boston, Amer. Meteor. Soc., Monograph 23, 43pp.

Ference, M., Jr., 1951: Instruments and techniques for meteorological measurements. Compendium of meteorology, Boston, Amer. Meteor. Soc., 1334pp.

Griffith, E. V., 1961: Polynomial curve fitting and evaluation. International Business Machines Corp., 11pp. (unpublished manuscript).

Howard, J. N., D. L. Burch and D. Williams, 1955: Near-infrared transmission through synthetic atmospheres. Geophys. Research Papers, No. 40, AFCRC-TR-55-213.

Kaplan, L. D., 1952: On the pressure dependence of radiative heat transfer in the atmosphere. J. Meteor., 9, 1-12.

Kaplan, L. D., 1954: The infrared spectrum of lower stratosphere and its importance in the heat balance, Scientific Proceedings of the International Union of Geodesy and Geophysics, Association of Meteorology, 10th General Assembly, Rome, Sept. 1954, London, 1956, 583-592.

Kuhn, P. M., 1961: Accuracy of the airborne economical radiometer., Mon. Wea. Rev., 89, 285-287.

Ladenburg, R., and F. Reiche, 1913: Ueber sele Ktive absorption., Ann. der Phy., 42, 181-203.

Lettau, H. H., and B. Davidson, 1957: Exploring the atmosphere's first mile. Pergamon Press, 162pp.

Lorentz, H. A., 1905: The absorption and emission lines of gaseous bodies. Proc. Acad. Amsterdam, 8, 591.

Manabe, S. and F. Moller, 1961: On the radioactive equilibrium and heat balance of the atmosphere. Mon. Wea. Rev., 89, 503-532.

Middleton, W. E. K., and A. F. Spilhaus, 1953: Meteorological Instruments. Univ. of Toronto Press, 286pp.

Moller, F., 1944: Grundlagen enes diagramms zur berechnung langwelliger strahlungsstrome. Meteor. Zeit., 61, 37-45.

Moller, F., 1944: Wirkungen der langwelligen strahlung in der atmosphare., Meteor. Zeit., 61, 264-270.

Robinson, G. D. 1950: Note on the measurement and estimation of atmospheric radiation. Quart. J. R. Meteor. Soe., 76, 37-51.

Suomi, V. E. and P. M. Kuhn, 1958: An economical net radiometer. Tellus, 10, 160-163.

Suomi, V. E., D. O. Staley and P. M. Kuhn, 1958: A direct measurement of infrared radiation divergence to 160 mb. Quart. J. R. Meteor. Soc., 84, 134-141.

Townes, C. H., and F. R. Merritt, 1946: Water spectrum near one-centimeter wavelength. Phys. Rev., 70, 558.

WINTERTIME ATMOSPHERIC INFRARED COOLING OVER THE CARIBBEAN AND THE UNITED STATES

BY

ROMEO RONNIE SABATINI

1962

ABSTRACT

Results of 170 radiometersonde ascents made in the United States and Caribbean area are presented. Average infrared fluxes and cooling rates are obtained and are compared with theoretical calculations. The observed infrared cooling rates differ most markedly from theoretical results in the upper troposphere, tropopause, and stratosphere. Relatively strong warming is noted centered at 175mb, and strong cooling is obtained above 100mb. The observations support calculations by Krishnamurti (1961) based on mass circulation requirements near the subtropical jet which indicate that warming should occur near 150mb. It is concluded that the layer centered at 175mb actually gains energy by infrared radiation and that it is necessary to modify present estimates of the energy transported to the upper troposphere by convection.

ACKNOWLEDGEMENTS

I am forever grateful to Doctor Verner E. Suomi who patiently guided me through this work with his helpful suggestions and his encouragement. My thanks also go to Doctor Peter M. Kuhn and Mr. Robert Bushnell.

This research was supported by the U. S. Weather Bureau under Contract CWB-9475.

Fig. 1. Location of stations. (Miami was included in the Caribbean network)

Fig. 2. Behavior of atmospheric infrared fluxes.

Fig. 3. Averages of infrared fluxes, cooling rates, and air temperature for the United States during December 1960-January 1961. All ascents

Fig. 4. Averages of infrared fluxes, cooling rates, and air temperature for the United States during December 1960-January 1961. Ascents made under clear skies.

Fig. 5. Averages of infrared fluxes, cooling rates, and air temperature for the United States during December 1960-January 1961. Ascents made with low and middle clouds overcast.

Fig. 6. Averages of infrared fluxes, cooling rates, and air temperature for the United States during December 1960-January 1961. Ascents made with cirrus overcast.

Fig. 7. Averages of infrared fluxes, cooling rates, and air temperature for the Caribbean during December 1960-January 1961. All ascents.

Fig. 8. Averages of infrared fluxes, cooling rates, and air temperature for the Caribbean during December 1960-January 1961. Ascents made under clear skies and 1/10 cumulus cover.

Fig. 9. Observed and calculated infrared cooling rates for middle latitudes.

Fig. 10. Observed and calculated infrared cooling rates for low latitudes.

INTRODUCTION

The heat budget of the atmosphere is made up of the infrared cooling, the solar heating, the net latent heating, the heating from the lower boundary, and the rate of heat storage (see Davis, 1961). A large part of this heat budget is the infrared cooling of the earth's atmosphere. Various investigators have attempted to calculate the contributions of these different processes to the heat budget. Particular attention has been given to the contribution of infrared cooling to this budget both in the lower and upper atmosphere (see for instance London, 1952,1956, 1957; Plass, 1956a, 1956b; Brooks, 1958; Ohring, 1958; Manabe and Moller, 1961; Davis, 1961). Their calculations are based on average atmospheric distributions of temperature, pressure, water vapor, carbon dioxide, and ozone. To make the picture more realistic, London and Davis included the effect of clouds in their model atmospheres.

The purpose of this study is to present results of actual measurements of the infrared fluxes and cooling through the atmosphere for the United States and Caribbean area during December 1960 and January 1961, and compare these with calculations based on theory and climatic means.

BEHAVIOR OF ATMOSPHERIC INFRARED RADIATION

The difference of the upward and downward flux of radiation is the net flux of radiation, F_{net}. The infrared cooling (or warming) is calculated from the divergence of F_{net} by

$$\frac{\Delta T}{\Delta t} = \frac{g}{C_p} \frac{\Delta F_{net}}{\Delta p} \qquad (1)$$

where $\frac{\Delta T}{\Delta t}$ is the infrared cooling; g the acceleration of gravity; Cp is .239 calories $g^{-1}C^{-1}$ the specific heat of air at constant pressure; ΔF_{net} is the net infrared flux difference for the pressure interval ΔP.

The infrared radiation from the earth's surface is partly lost to space through the atmospheric window and partly absorbed and re-emitted downward and upward by atmospheric absorbers. The most important absorbers of infrared radiation in the atmosphere are water vapor, carbon dioxide, ozone, and particulate matter. The downward flux of infrared radiation (F_{down}) at any level i in the atmosphere is the sum of the partial contributions to this flux by the individual absorbers. This contribution from each absorber is

$$F_i = \int_0^u \sigma T^4(u) \frac{\partial \epsilon_f(u)}{\partial u} du \qquad (2)$$

where u is the optical thickness of the absorber; σ is the Stefan-Boltzmann constant; ϵ_f is flux emissivity; T is the mean temperature of the layer of optical thickness du.

To the upward flux (F_{up}) a term is added for the transmitted radiation from the earth's surface. The transmitted term is higher with higher surface temperatures and with lower concentrations of atmospheric absorbers. Theoretical calculations of the infrared fluxes are based on equation (2). For a more complete explanation and treatment of equation (2) see for example Elsasser (1942). From equation (2) it is seen that the infrared fluxes in the atmosphere are intimately related to the kind of absorbers, their concentrations, temperatures, and emissivities. It is therefore of the utmost importance to have accurate measurements of these quantities in the atmosphere in order to calculate the infrared fluxes.

Figure 2 illustrates the behavior of the infrared fluxes in the atmosphere for different absorbers' concentrations and temperature distributions. In figure 2a both temperature and absorbers' concentrations decrease with height. Generally the upward flux decreases with height but less rapidly as we go higher because the absorbers' concentration decreases. The downward flux, which is zero at the top, increases slowly in the upper portions, progressively more rapidly in the lower portions, to a maximum at the ground. The net flux through this atmosphere is everywhere directed outward; it is small near the surface and large at the top, resulting in a net flux divergence (i.e., cooling). If temperatures increase with height and absorbers' concentration decrease (upper

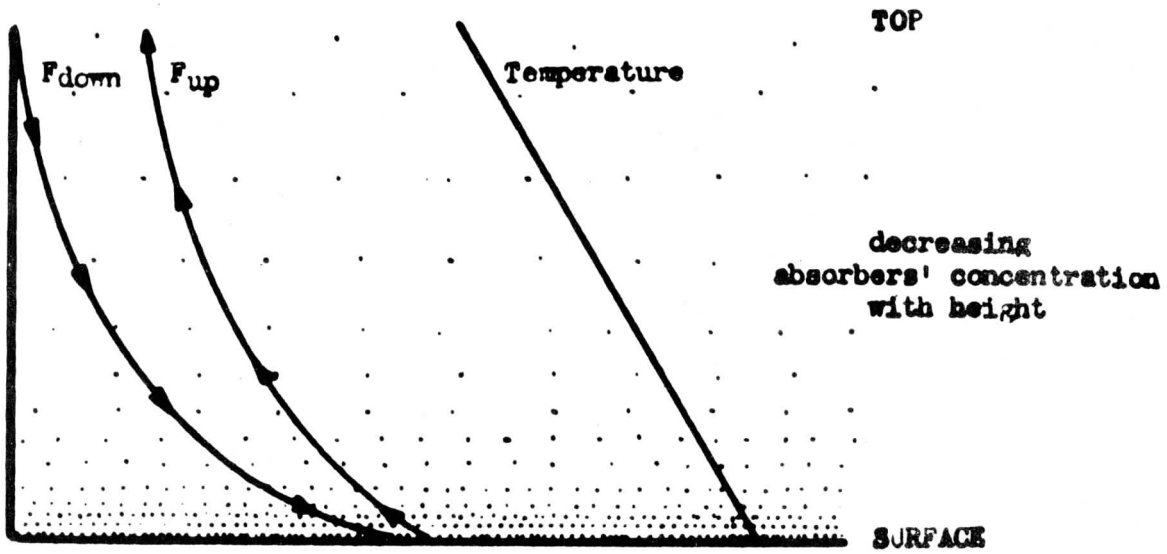

Figure 2a

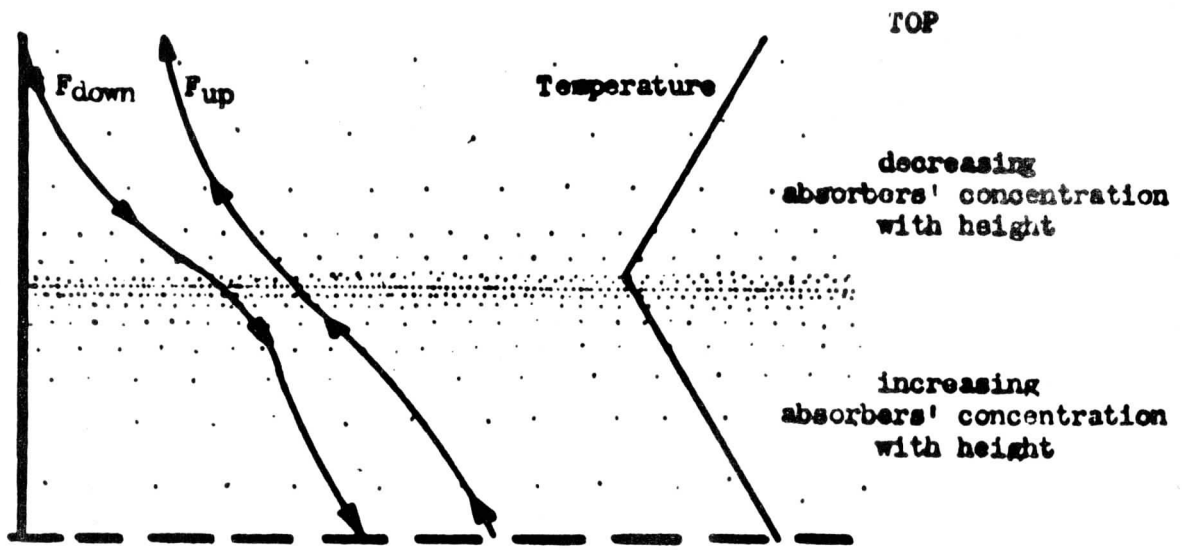

Figure 2b

Fig. 2. Behavior of atmospheric infrared fluxes.

part of figure 2b) rapidly, we would still obtain a high upward flux at the top, and therefore a large flux divergence. If in an atmospheric layer the concentrations of the absorbing gases, and/or particulate matter, increase with height (lower part of figure 2b), causing a decrease in atmospheric transmissivity, the net flux in the upper portions is made smaller and this can result in a net flux convergence (i.e., warming).

Thus it is theoretically possible to calculate the atmospheric infrared fluxes, but the calculations are not reliable because measurements of atmospheric absorbers, especially in the upper troposphere and above, are inadequate. It is therefore most desirable to measure the infrared fluxes through the atmosphere directly. The Suomi-Kuhn radiometer is well adapted for this purpose. It is cheap, fairly accurate, and can be easily attached to the standard U. S. Weather Bureau radiosonde. The combination of radiosonde and radiometer is known as radiometersonde. This study will present results from 170 such radiometersonde ascents made in a regular radiosonde network.

DATA PROCESSING

A total of 170 radiosondesonde ascents made at various stations in the United States and Caribbean area (figure 1) during the months of December, 1960 and January, 1961 were used for this study. The upward (F_{up}) and downward (F_{down}) fluxes of infrared radiation were measured through the atmosphere by means of the Suomi-Kuhn radiometer (Suomi and Kuhn, 1958) attached to the standard U. S. Weather Bureau radiosonde. The fluxes were averaged at every 25mb up to 100mb, and at every 10mb beyond 100mb. The average cooling for a layer in degrees Celsius per day was then obtained from the average net radiation flux (F_{net}) by means of equation (1) which reduces to

$$\frac{\Delta T}{\Delta t} = -5904.6 \frac{\Delta F_{net}}{\Delta P}$$

where $\frac{\Delta T}{\Delta t}$ is the infrared cooling in degrees Celsius per day; ΔF_{net} is the net infrared flux difference in langleys per minute for a change in pressure ΔP in millibars. The cooling was calculated for 50mb layers up to 100mb, and for 20mb layers above 100mb. The calculations were done with the aid of the CDC 1604 of the

RADIATION CHARACTERISTICS OF THE TROPOSPHERE

The infrared cooling for the entire troposphere is greatest in the Caribbean region (Fig. 7) because of the high water temperatures and the corresponding high water vapor content of the lower troposphere. The average for all the United States flights (Fig. 3) shows little cooling near the surface because of the high occurrence of low clouds causing a high back radiation from the cloud deck and low values of both F_{net} near the ground and ΔF_{net} for the layer extending from the surface to the average low cloud bases. The average tropopause height was 99mb for the Caribbean, and 238mb for the United States. The average infrared cooling rate from 1000mb to 100mb for the Caribbean is 1.34°C per day, while for the United States it is .98°C per day from 975mb to 250mb. The tropical troposphere therefore, on the average loses about 70 percent more energy by infrared cooling than the middle latitudes troposphere when the additional thickness of the tropical troposphere is taken into account. The Caribbean average shows the largest infrared cooling for the whole atmosphere (1000mb-30mb) being 1.46°C per day as compared to .95°C per day for the United States (975mb-30mb). The cooling for the Caribbean shows a maximum in the troposphere at the 725mb, just above the average height of the tops of cumulus clouds, the predominant type of clouds in the tropics. The cooling for the United States shows a slight maximum in the troposphere at the 825mb level and a very gradual decrease toward the tropopause and an abrupt

decrease at 300mb.

Figures 9, 10, and Table 3 compare the observed infrared cooling rates through the atmosphere with those calculated by London (1957), Davis (1961), Manabe and Moller (1961), and Krishnamurti (1961). London and Davis assumed average cloud cover. Manabe and Moller calculated the contributions of water vapor, carbon dioxide, and ozone to the infrared cooling. The total infrared cooling curve for Manabe and Moller shown in Fig. 9 was obtained by adding graphically these partial contributions. However, their calculations are for clear skies for the year and for the whole Northern Hemisphere. Krishnamurti calculated his infrared cooling rate requirements from mass circulations for 37N to 17N, at the mean position of the winter subtropical jet. All the calculated averages of the infrared cooling are for latitude bands, while our observed averages are for the United States and Caribbean area only. Our comparisons of the calculated and the observed infrared cooling rates should be taken with this point in mind.

The observations clearly show that the calculated cooling rates are overestimated in the upper troposphere and tropopause region, and underestimated in the stratosphere (see Figs. 9, 10, and Table 3). London's infrared cooling for the low troposphere are overestimated. Although his values for 20N are almost exactly the same as the observations for the Caribbean, the actual cooling

averaged around the earth in low latitudes should be lower than what it is observed in the Caribbean, since the cooling in the Caribbean is emphasized by the warm water currents in this region. Krishnamurti's cooling rates for the lower atmosphere are underestimated. He calculated his cooling rates from mass circulation requirements and did not consider the additional cooling required to balance the heat released by condensation in the troposphere, hence his values are lower than the observations. Davis and Manabe and Moller's cooling rates for the lower atmosphere are closer to the observations. Manabe and Moller's curve shows a cooling rate of 1.4 day^{-1} for the 975mb-500mb layer as compared to 1.2°C day^{-1} for the same layer, for the observed clear United States average in December-January (Table 1).

The average cooling rates for the clear troposphere for both the United States (Fig. 4) and Caribbean (Fig. 8) show a gradual decrease from the middle troposphere to the tropopause region. Since there were only very few ascents made with totally clear sky conditions in the Caribbean, the ascents made under one tenth cumulus cover were included in the Caribbean clear average. This accounts for a cooling minimum centered at 875mb corresponding approximately to the average bases of the cumulus clouds.

The average for the low and middle clouds overcast for the United States (Fig. 5) had about the same cooling rate for the troposphere as the clear average (1.11°C per day as compared to

1.12°C per day for the clear average), but a different cooling distribution. Since a decrease in cooling is expected below a cloud deck and an increase above it, one would attempt to relate the maxima and minima of cooling observed in figure 5 to low, middle and high clouds. Although these maxima and minima of cooling above and below clouds are clearly brought out in individual soundings, they tend to smooth out in an average because of the variable cloud heights. Nevertheless, the minimum of cooling at 525mb is sharp enough to warrant consideration, and would correspond to the average height of middle clouds in temperate latitudes. The small cooling rates near the surface are probably due to low clouds trapping in the infrared radiation. Although the net radiation curves for both the clear and low and middle clouds overcast averages have about the same slope in the troposphere (975mb-250mb), hence giving about the same cooling rates for both, the net radiation through the atmosphere for overcast is depleted. This results from the fact that at the ground F_{net} is made small by the large back radiation of the low cloud bases which are at a temperature close to the ground temperature, and higher up F_{net} is decreased because the high cloud tops act as a black radiator with low radiating temperature.

The presence of cirrus strongly depletes the infrared cooling in the troposphere. In the case of cirrus overcast both the tops and bottoms of the cirrus have very low radiating temperatures,

hence F_{net} at the top of the troposphere is decreased much more than F_{net} at the ground, reducing the slope of F_{net} and therefore lessening the cooling rate in the troposphere. The average cooling rate for the troposphere (975mb-250mb) for the cirrus overcast (Fig. 6) is .80°C per day, about 30 percent less than for the clear or low and middle clouds average.

RADIATIVE PROPERTIES OF THE TROPOPAUSE AND STRATOSPHERE

The greatest discrepancy between the observed and the theoretically calculated infrared cooling rates is near the tropopause and in the stratosphere. Possibly this is because the concentrations of the infrared absorbers are not well known at these heights. The standard radiosonde hygristor does not function properly below -40°C and there are few soundings made with frost point hygrometers or other accurate moisture measuring devices. Only a few measurements of ozone and particulate matter are available for this region also.

Although London (1952, 1957), Davis (1961), and Manabe and Moller (1961) showed a decrease in cooling toward the level of the tropopause in their model atmospheres (see Figs. 9, 10, and Table 3) they did not obtain the relatively strong warming observed in this region.

It is most interesting to notice that Krishnamurti (1961) obtained warming above 150mb. He arrived at his cooling rates indirectly from mass circulation requirements for 37N-17N at the mean position of the subtropical jet.

The observed cooling rates decrease rapidly toward the tropopause for all averages. In the United States average (Fig. 3) a warming maximum of 0.45°C per day is noted at 175mb above the average height of the winter tropopause. The Caribbean average shows (Fig. 7) lesser warming of 0.35°C per day also centered at about 175mb below the average height of the tropical tropopause.

The warming in the Caribbean is confined to the 200mb to 150mb layer, while it extends from 250mb to 100mb in the United States average. This warming near the tropopause has already been noticed by Kuhn et. al., (1959, 1960) and Darkow (1960) from radiometer measurements through the atmosphere. Staley (1958) suggested that the tropopause temperature minimum is not due to radiative processes since he calculated that radiative transfer would cause warming at the temperature minimum and hence would act to increase the temperature at the tropopause. From the observations we see that this warming is present near the tropopause in the United States and hence available to heat this region, but it is not present near the tropical tropopause except for the clear sky average (Fig. 8). In all averages except the tropical clear sky average and possibly the United States cirrus average (Fig. 6) this warming occurs below and not at the temperature minimum as Staley suggested. Manabe and Moller (1961) stress the importance of the increased downward long wave radiation by the water vapor in the stratosphere in causing the cooling minimum they obtained near the tropopause in their model atmosphere. Goody (1949), Plass, (1956) and Manabe and Moller also find that the 15 micron band of carbon dioxide causes a relative warming trend near the tropopause. Kuhn and Suomi (1959) and Manabe and Moller (1961) mention the possibility that the warming in the tropopause region may be due to the absorption in this region of radiation from the region of high

temperature high in the stratosphere at about 50km and from the warmer troposphere below.

The observed warming by infrared radiation centered at 175mb is equivalent to an energy addition to the layer 200mb to 150mb of 0.11 calories per gram of air per day for the December-January United States average, and 0.09 calories per gram of air per day for the December-January Caribbean average. A survey of the infrared cooling in the Caribbean by us and by Riehl (1962) who used our same data for the months of October and November, 1960 showed a greater warming rate around the 175mb region than for December, 1960 and January, 1961. This corresponded to double the amount of energy added to the air by infrared radiation in this region. Table 4 gives a summary of the energy added to the layers that are warmed by infrared radiation. As one can see from Table 4, this warming in the Caribbean decreased both in depth and intensity from October, 1960 to January, 1961. Infrared radiation is therefore a source of energy near the tropopause and lower stratosphere region. This indicates that energy transported upwards by convection is less important than previously thought.

Although the Suomi-Kuhn radiometer is most reliable in the troposphere (Bushnell, 1961; Kuhn, 1961) it has greater errors in the stratosphere. The averaging process should tend to minimize them, but the results for the stratosphere should not be considered as reliable.

In the stratosphere the temperature generally increases with height, while the more important absorber concentrations decrease rapidly with height, thus it follows from the previous qualitative discussion that large infrared cooling rates should be observed. In all cases strong cooling was obtained above 100mb, slightly greater at higher latitudes, averaging 3.17°C per day for all the United States flights for the 100mb to 30mb layer, and 3.02°C per day for all the Caribbean flights for the same layer. Ohring (1958), Brooks (1958), and Manabe and Moller (1961) obtained a cooling rate of about 2°C per day and increasing upwards in the stratosphere due to the carbon dioxide and water vapor. They account this cooling to the high transmissivities of carbon dioxide in the stratosphere and the rapid decrease of water vapor with height. These two factors combined cause a rapid increase in the net flux with height resulting in a large flux divergence (i.e., strong cooling). Plass (1956) finds a cooling rate of 2 to 3°C per day, but higher up at 30km to 60km. He suggests that the 14 micron band of O_3 may contribute substantially to the cooling at these heights. Both London (1957) and Davis (1961) obtained cooling in the stratosphere, but much smaller than observed. Davis stresses the importance of the rotational band of water vapor at these heights as the major contributor to this cooling.

Experiments are now being carried out at the University of Wisconsin by Bushnell (1962) and Kuhn (1962) to check thoroughly

the performance of the Suomi-Kuhn radiometer in the stratosphere. Preliminary results tend to confirm the high cooling rates observed.

CONCLUSION

Observations show that infrared cooling rates calculated from climatic means have been overestimated in the upper troposphere and tropopause region, and underestimated in the stratosphere.

Krishnamurti's calculated infrared warming requirements above 150mb from mass circulation around the subtropical jet is roughly in agreement with the observed warming at 175mb.

Except for the clear (1/10 cumulus) Caribbean average, and possibly the United States cirrus average, the warming maximum does not occur at the temperature minimum near the tropopause.

As a consequence of the observations which show that present infrared cooling rates have been overestimated in the upper troposphere it follows that energy transported upwards by convection is less than previously thought and that radiation has a greater stabilizing influence on the atmosphere than previously thought.

Cirrus clouds strongly diminish the tropospheric cooling.

Although this study brought out interesting features of the infrared fluxes and cooling especially in the less known regions of the tropopause and stratosphere it is by no means a complete climatological survey. This is what has been observed for a particular winter for the United States east of the Rockies and for the Caribbean area. Will warming near 175mb be present for example over Europe, on the eastern side of the Bermuda High, or over the Atlantic and

Pacific Ocean? How does the atmospheric cooling (and warming) vary with season? Preliminary studies indicate that warming near 175mb is greater in the fall than in winter at least for the Caribbean, and is not present over the Antarctic.

In the long run satellite observations of infrared radiation may eventually provide good estimates of the total atmospheric infrared cooling over the whole world (Sabatini and Suomi, 1962), a feat which is out of the question by using only net radiometers attached to balloons. Nevertheless, an obvious advantage of the balloon-borne radiometer is that it gives a profile of the fluxes through the atmosphere, while the satellite of course, can only give the value of the outgoing flux at the top of the atmosphere.

Table 1

Infrared cooling rates in C day^{-1} for the United States

Layer mb	Clear	Overcast	Overcast Cirrus	All Ascents
975-900	.91	.75	.46	.73
900-850	1.41	.86	1.39	1.29
850-800	1.31	1.50	1.48	1.30
800-750	1.15	1.35	1.25	1.17
750-700	1.50	1.15	1.18	1.20
700-650	1.23	1.26	.78	105
650-600	1.41	1.22	.59	1.16
600-550	1.36	1.09	.78	1.05
550-500	1.56	.64	.78	1.15
500-450	1.22	1.45	.54	1.00
450-400	1.04	1.25	.44	.90
400-350	1.00	1.74	.63	.91
350-300	.47	1.45	.92	.76
300-250	.26	.04	.28	.21
250-200	-.30	.25	-.45	-.17
200-150	-.58	-.37	-.77	-.45
150-100	-.22	.06	1.05	-.05
100- 80	1.42	1.74	.03	1.24
80- 60	2.63	2.39	1.27	1.39
60- 40	4.05	6.47	2.95	5.05
975-500	1.29	1.07	.93	1.10
500-250	.79	1.18	.56	.75
250-100	-.36	-.02	-.05	-.22
100- 30	3.12	4.48	2.24	3.17
975- 30	1.03	1.18	.77	.95

Table 2

Infrared cooling rates in C day^{-1} for the Caribbean region

Layer mb	Clear (1/10 Cu)	All ascents
1000-950	2.96	1.95
950-900	2.17	1.67
900-850	1.77	1.57
850-800	2.24	1.89
800-750	2.09	2.15
750-700	2.35	2.28
700-650	2.11	2.18
650-600	1.82	1.67
600-550	1.75	1.51
550-500	1.54	1.46
500-450	1.28	1.35
450-400	1.11	1.10
400-350	.99	.92
350-300	.70	.57
300-250	.47	.59
250-200	.35	.64
200-150	-.10	-.35
150-100	.12	.78
100-80	-.68	2.45
80-60	2.60	2.98
60-40	1.95	3.13
1000-500	2.08	1.86
500-250	.89	.90
250-100	.12	.35
100-30	1.83	3.02
1000-30	1.45	1.46

Table 3

Observed and calculated infrared cooling in C day^{-1}

Layer mb	Observed U. S. Dec-Jan	London 40N winter	Davis 30-50N winter	Manabe and Moller N. H. Annual
975-500	1.10	1.7	1.2	1.4
500-250	.75	1.0	1.2	1.5
250-100	-.22	.5	.7	1.2
100-30	3.17	-	.8	.8

Layer mb	Observed Caribbean Dec-Jan	London 20N winter	Davis 20-30N Jan	Krishnamurti 17-37N winter
1000-500	1.86	1.9	1.5	.7
500-250	.90	1.4	1.7	1.4
250-100	.35	.8	.8	.8
100-30	3.02	-	.24	-

Table 4

Energy added to atmospheric layers by infrared warming in calories per gram of air per day

	Caribbean		United States
Layer mb	Oct-Nov	Dec-Jan	Dec-Jan
250-200	.04	-.16	.04
200-150	.20	.09	.11
150-100	-.14	-.20	.01

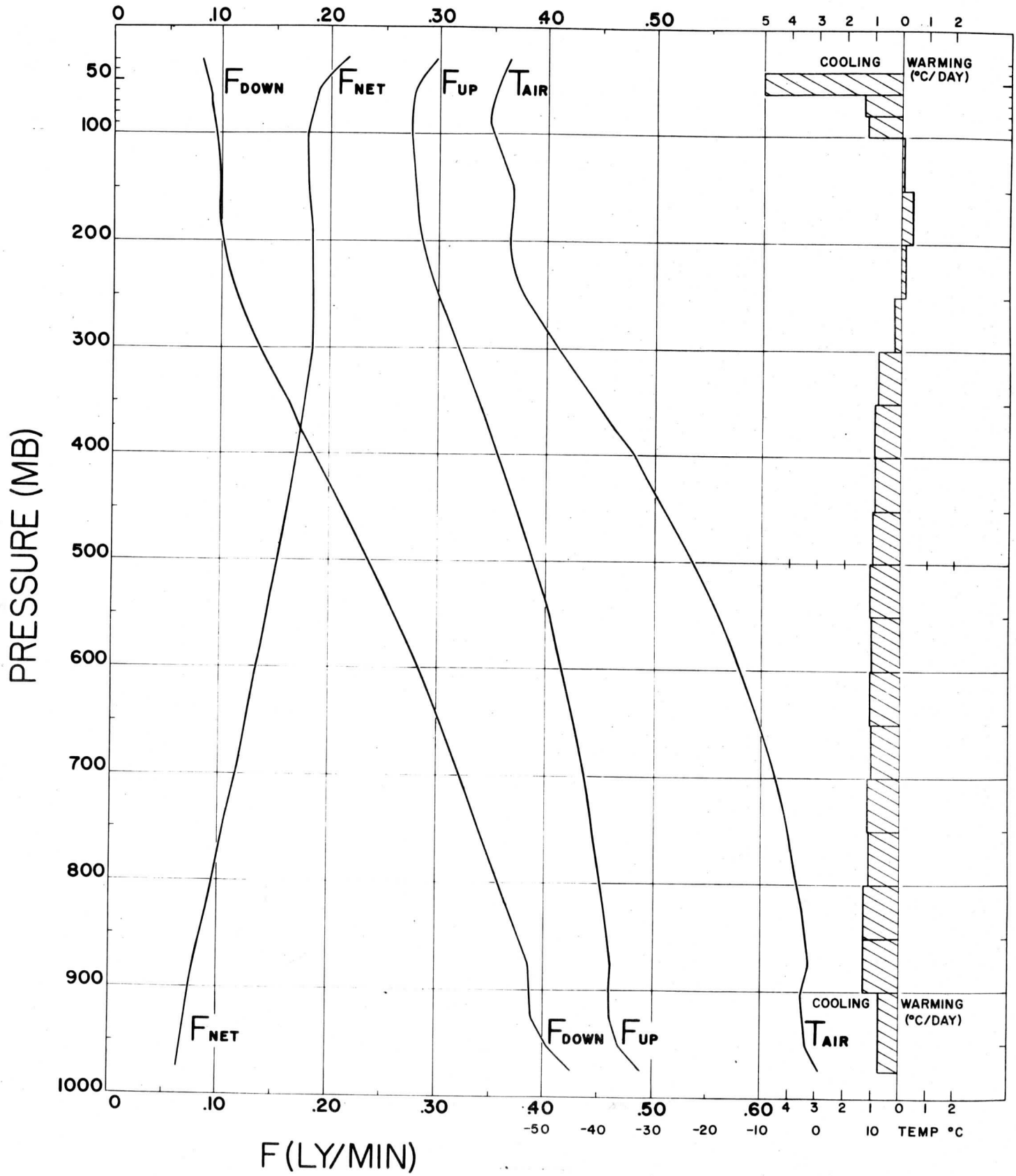
0 .10 .20 .30 40 .50
5 4 3 2 1 0 1 2
COOLING WARMING (°C/DAY)
F_{DOWN}
F_{NET}
F_{UP}
T_{AIR}
50
100
200
300
400
500
600
700
800
900
1000
PRESSURE (MB)
F_{NET}
F_{DOWN} F_{UP}
COOLING WARMING (°C/DAY)
T_{AIR}
0 .10 .20 .30 .40 .50 .60
4 3 2 1 0 1 2
-50 -40 -30 -20 -10 0 10 TEMP °C
F (LY/MIN)

Figure 3.

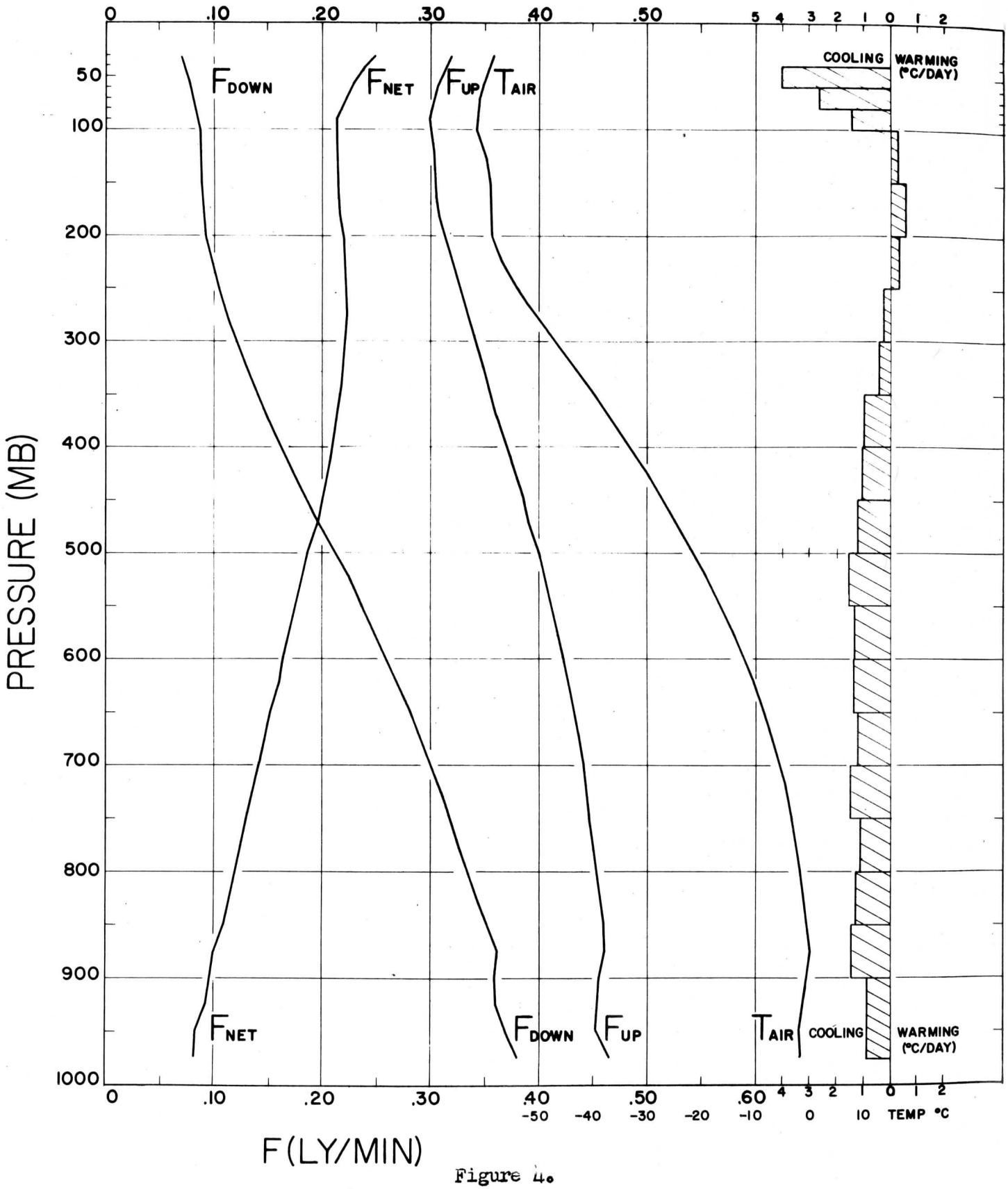
vs clear
0
.10
.20
.30
.40
.50
5 4 3 2 1 0 1 2
COOLING WARMING (°C/DAY)
F_DOWN
F_NET
F_UP
T_AIR
50
100
200
300
400
500
600
700
800
900
1000
PRESSURE (MB)
F_NET
F_DOWN
F_UP
T_AIR
COOLING
WARMING (°C/DAY)
0
.10
.20
.30
.40
.50
.60
4 3 2 1 0 1 2
-50
-40
-30
-20
-10
0
10
TEMP °C
F(LY/MIN)

Figure 4.

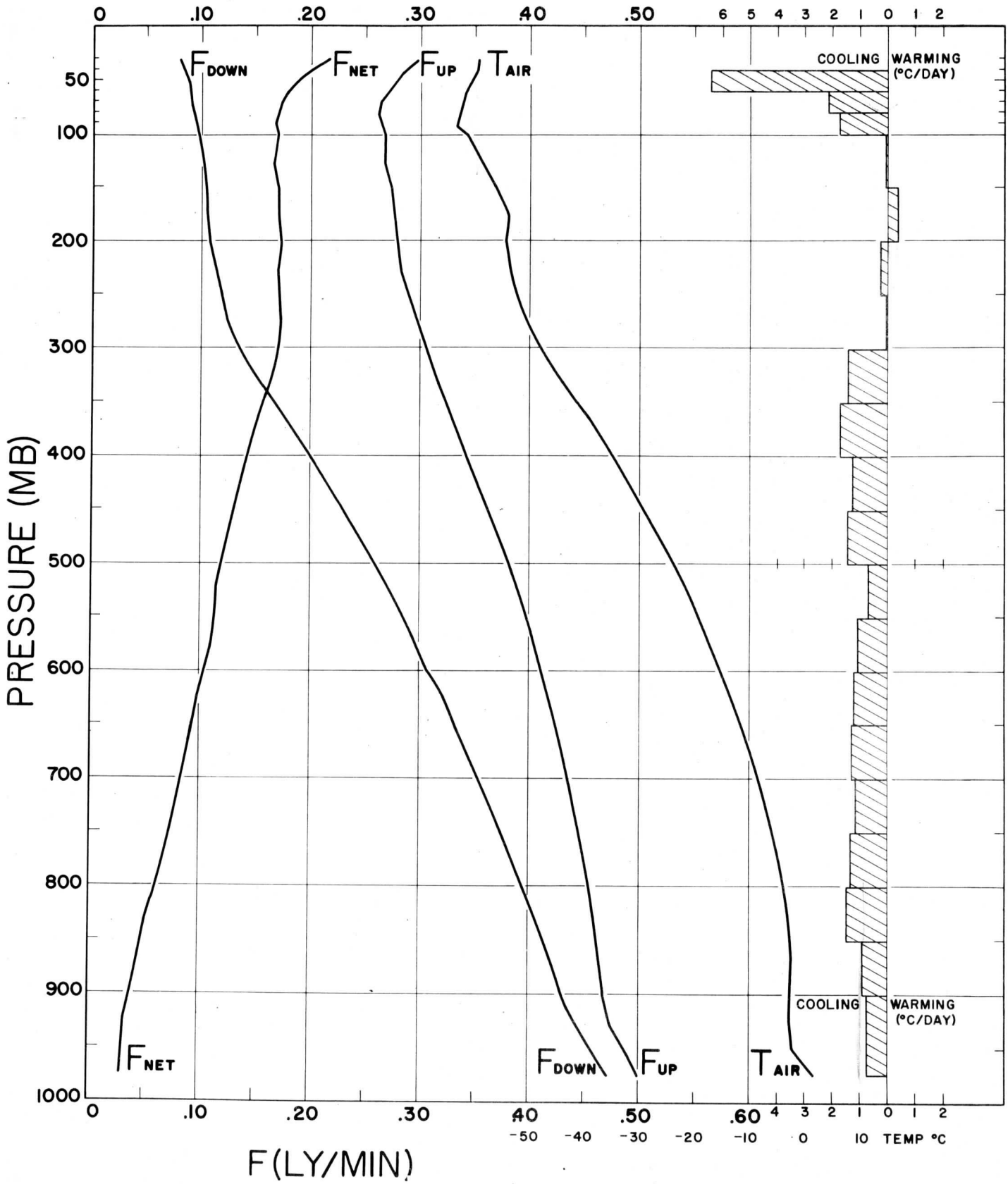
0 .10 .20 .30 .40 .50
6 5 4 3 2 1 0 1 2
COOLING WARMING (°C/DAY)
F DOWN
F NET
F UP
T AIR
50
100
200
300
400
500
600
700
800
900
1000
PRESSURE (MB)
F NET
F DOWN
F UP
T AIR
COOLING WARMING (°C/DAY)
0 .10 .20 .30 40 .50 .60
4 3 2 1 0 1 2
-50 -40 -30 -20 -10 0 10 TEMP °C
F(LY/MIN)

Figure 5.

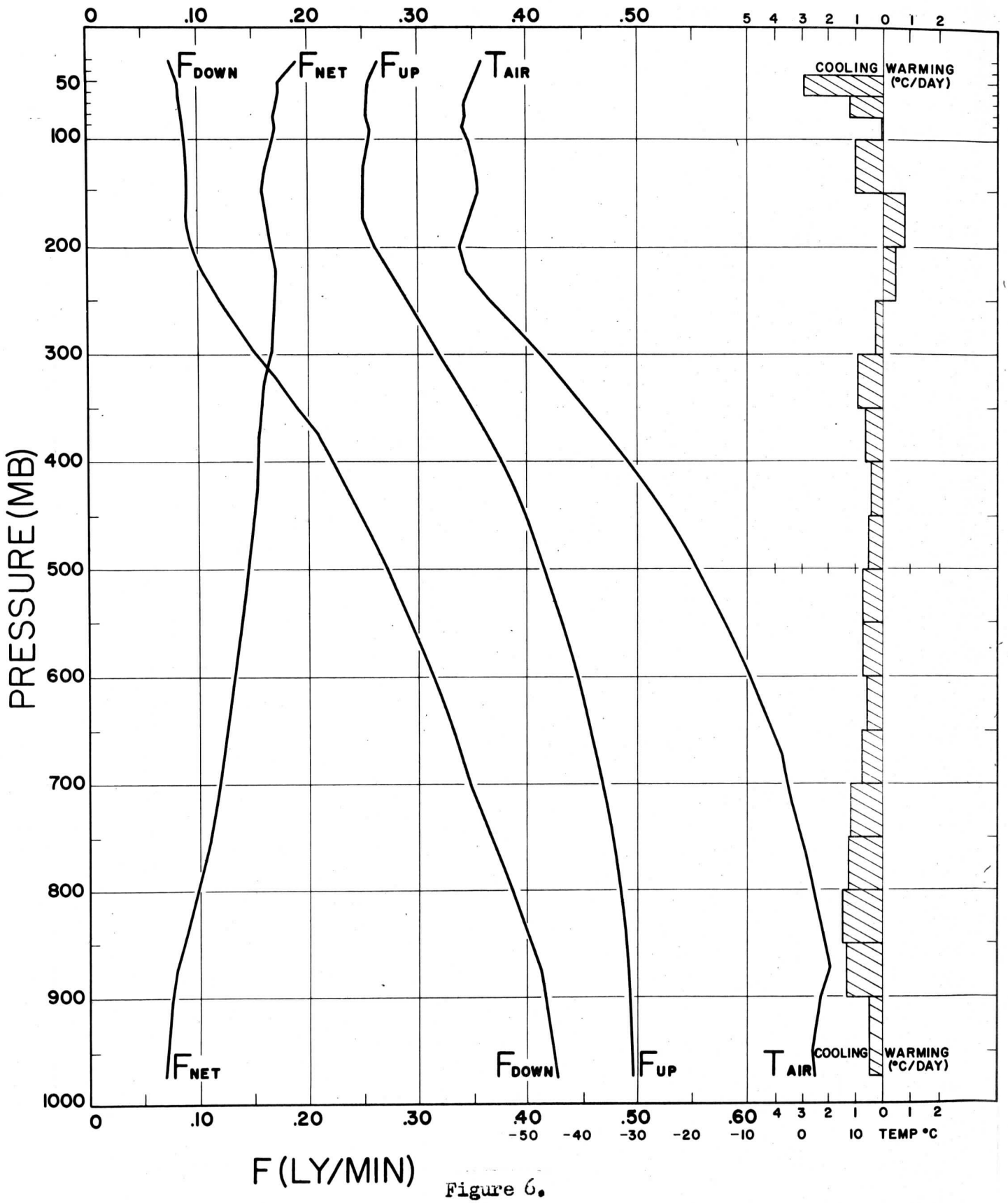
0 .10 .20 .30 .40 .50
5 4 3 2 1 0 1 2
COOLING WARMING (°C/DAY)
F DOWN
F NET
F UP
T AIR
PRESSURE (MB)
50
100
200
300
400
500
600
700
800
900
1000
F NET
F DOWN
F UP
T AIR
COOLING WARMING (°C/DAY)
0 .10 .20 .30 .40 .50 .60
-50 -40 -30 -20 -10 0 10 TEMP °C
F (LY/MIN)

Figure 6.

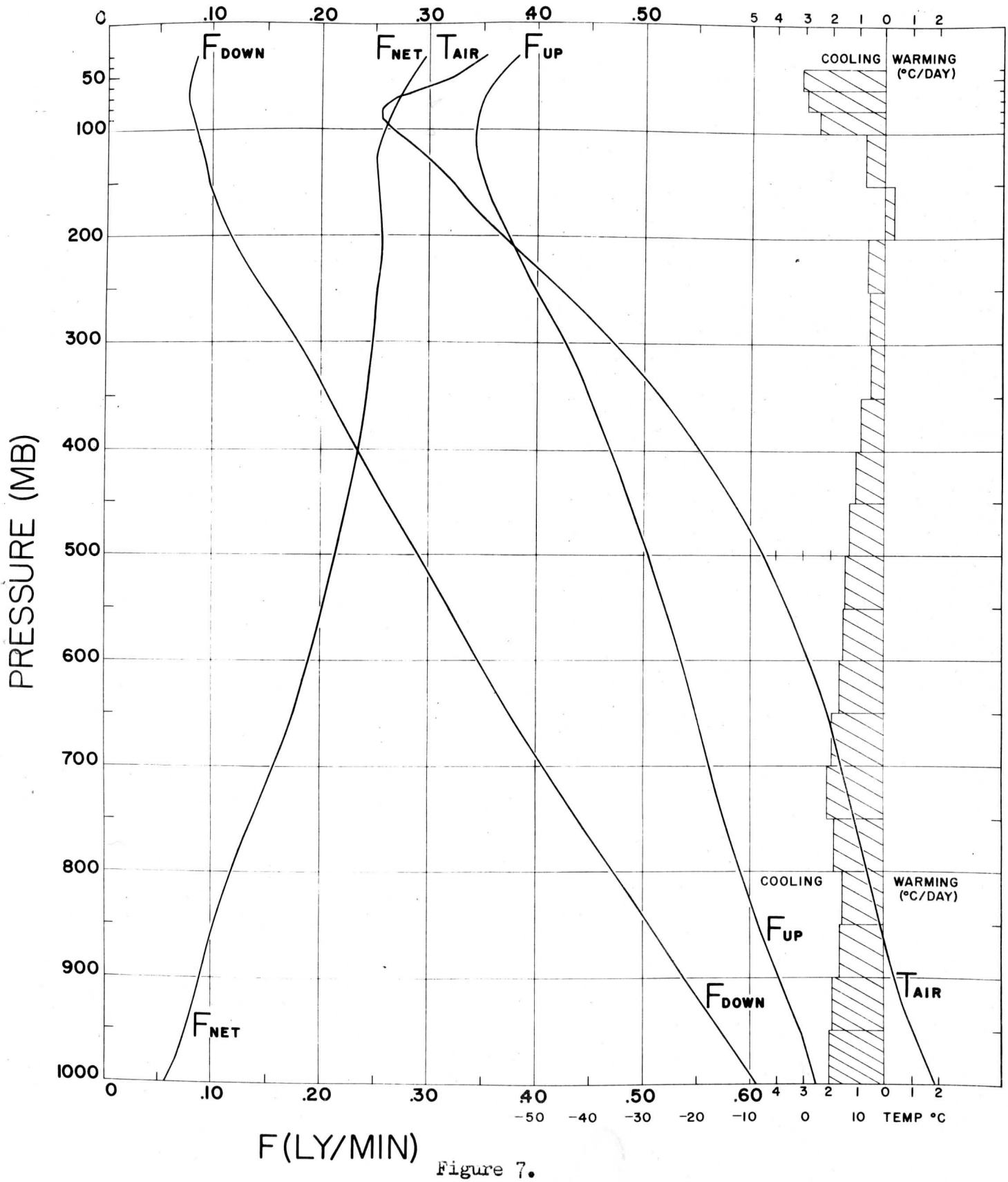
PRESSURE (MB)
F(LY/MIN)
TEMP °C
F DOWN
F NET
T AIR
F UP
COOLING
WARMING
(°C/DAY)
COOLING
WARMING
(°C/DAY)
F UP
F DOWN
T AIR
F NET
0
.10
.20
.30
.40
.50
.60
50
100
200
300
400
500
600
700
800
900
1000
5 4 3 2 1 0 1 2
4 3 2 1 0 1 2
−50 −40 −30 −20 −10 0 10

Figure 7.

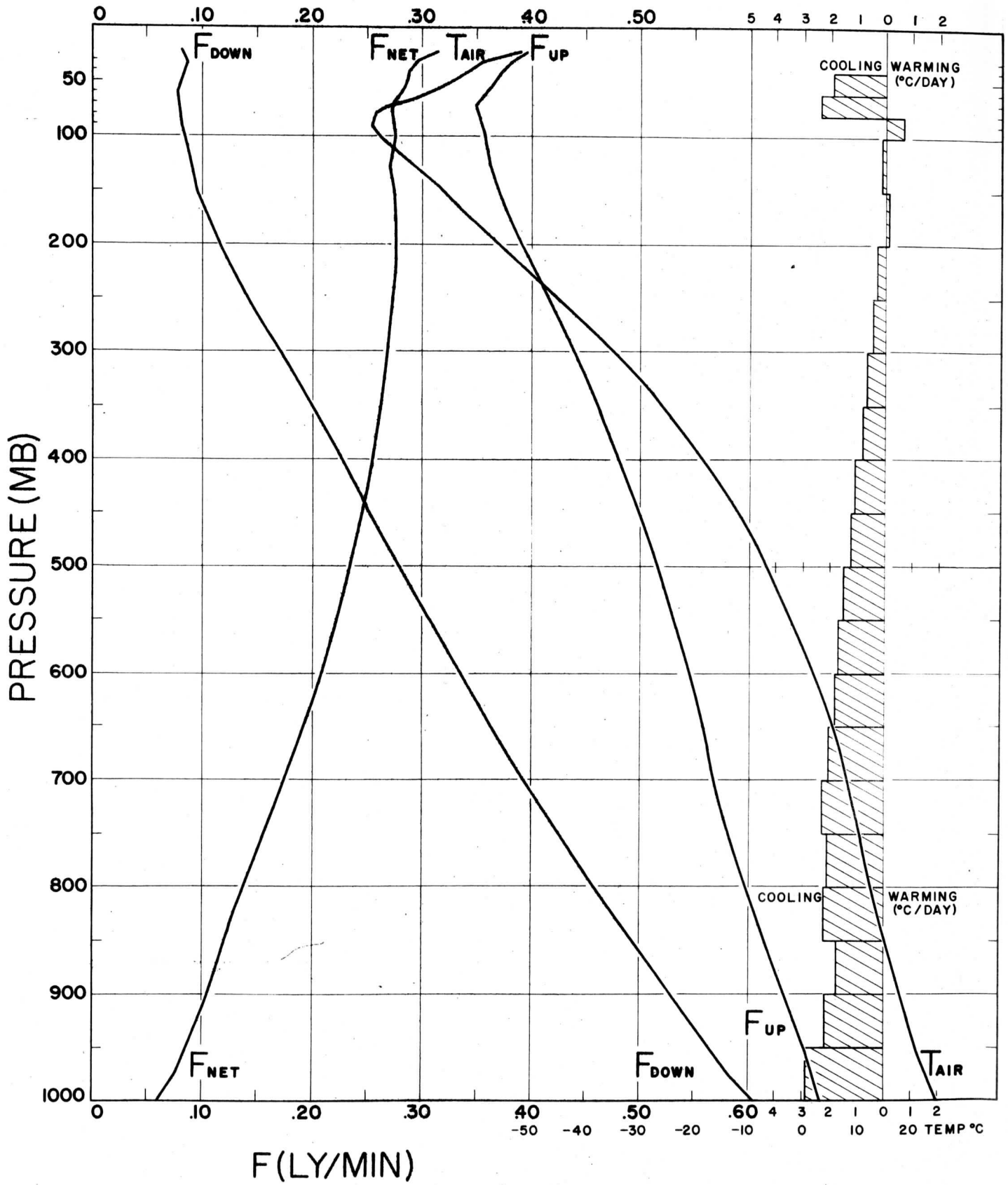
0 .10 .20 .30 .40 .50
5 4 3 2 1 0 1 2
F DOWN
F NET
T AIR
F UP
COOLING WARMING (°C/DAY)
50
100
200
300
400
500
600
700
800
900
1000
PRESSURE (MB)
COOLING
WARMING (°C/DAY)
F NET
F DOWN
F UP
T AIR
0 .10 .20 .30 .40 .50 .60
4 3 2 1 0 1 2
-50 -40 -30 -20 -10 0 10 20 TEMP °C
F(LY/MIN)

Figure 8.

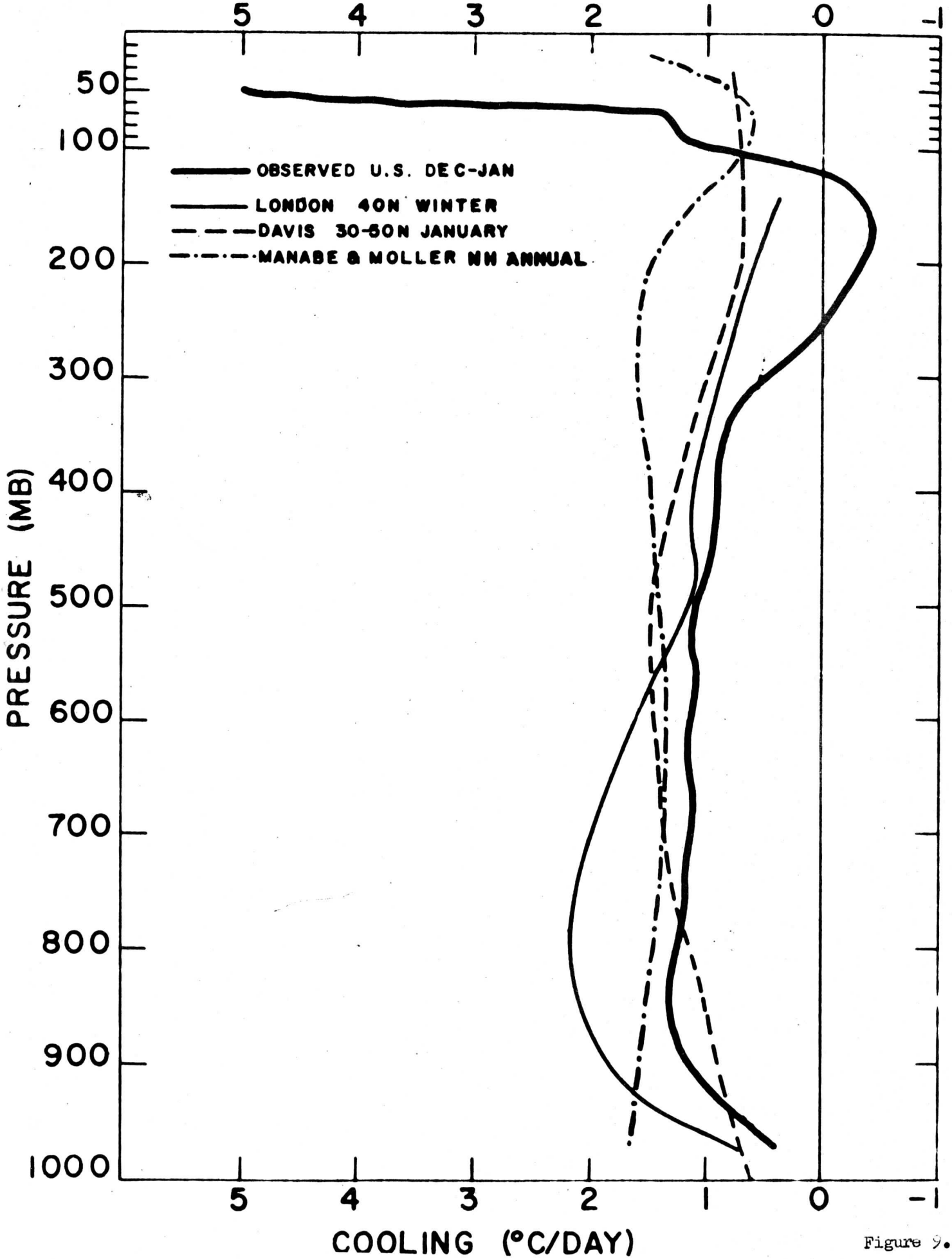
5
4
3
2
1
0
-1
50
100
200
300
400
500
600
700
800
900
1000
PRESSURE (MB)
OBSERVED U.S. DEC-JAN
LONDON 40N WINTER
DAVIS 30-50N JANUARY
MANABE & MOLLER NH ANNUAL
COOLING (°C/DAY)

Figure 9.

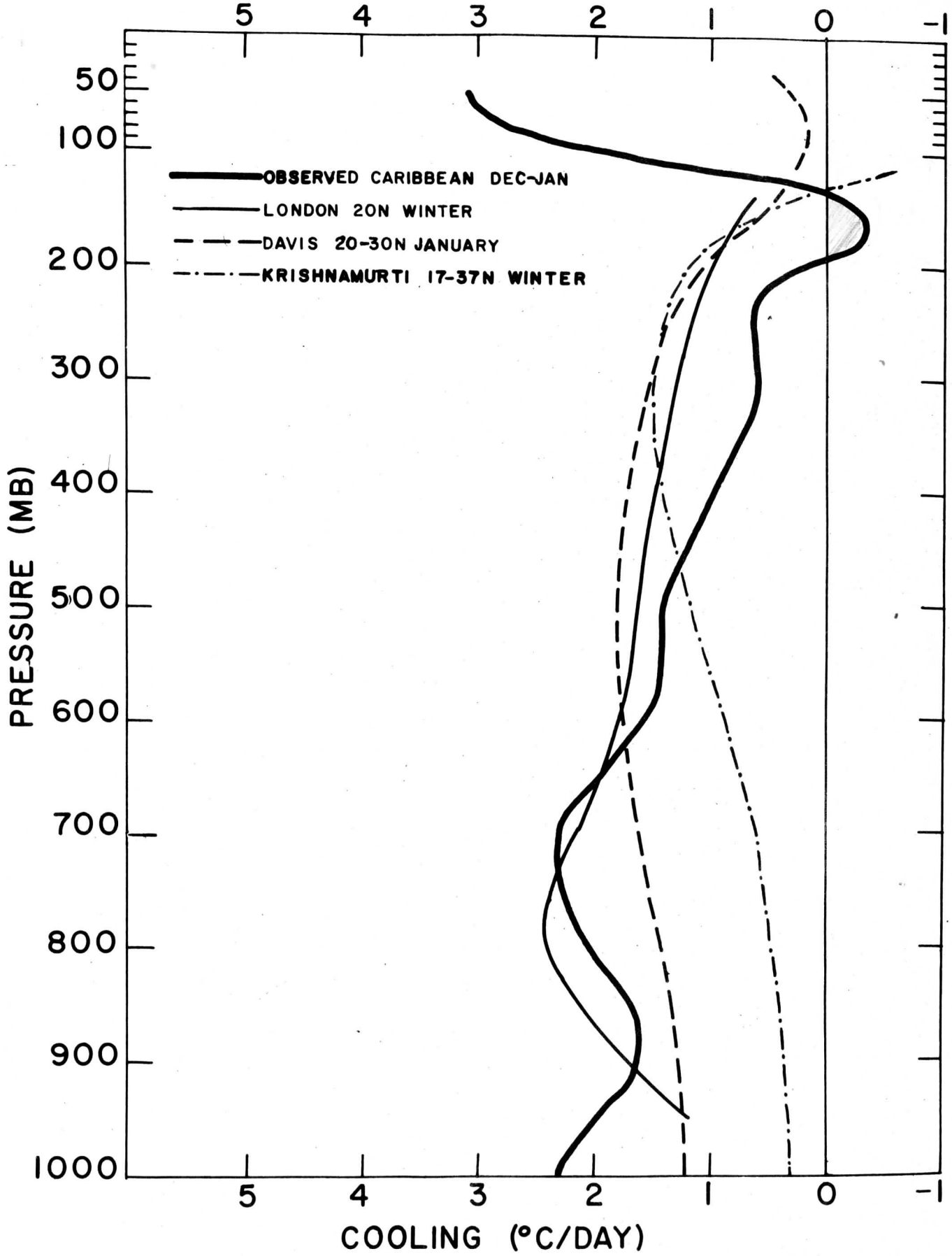

Figure 10. Observed and calculated atmospheric infrared cooling rates for low latitudes.

APPENDIX

Summary of averaged infrared fluxes in langleys per minute, and air temperature (T_{air}) in degrees Celsius. Pressure is in millibars.

United States December-January All Ascents

Pressure	F_{down}	F_{up}	F_{net}	T_{air}
975	.4252	.4895	.0642	.7
950	.4019	.4682	.0663	-1.9
925	.3897	.4605	.0708	-2.4
900	.3825	.4560	.0735	-2.4
875	.3857	.4635	.0778	-1.3
850	.3754	.4599	.0844	-1.9
825	.3662	.4559	.0897	-2.7
800	.3571	.4525	.0954	-3.6
775	.3483	.4489	.1006	-4.7
750	.3395	.4449	.1053	-5.2
725	.3305	.4409	.1104	-6.2
700	.3218	.4373	.1155	-7.5
675	.3127	.4326	.1199	-8.9
650	.3030	.4275	.1244	-10.5
625	.2935	.4219	.1284	-12.1
600	.2818	.4160	.1342	-14.0
575	.2711	.4098	.1387	-15.9
550	.2605	.4037	.1431	-18.1
525	.2494	.3971	.1476	-20.3
500	.2363	.3892	.1528	-22.8
475	.2242	.3814	.1571	-25.4
450	.2115	.3729	.1613	-28.2
425	.1988	.3645	.1657	-31.1
400	.1867	.3556	.1689	-33.7
375	.1728	.3466	.1737	-37.4
350	.1616	.3383	.1766	-40.7
325	.1489	.3292	.1803	-44.2
300	.1363	.3194	.1830	-47.8
275	.1254	.3100	.1845	-51.0
250	.1148	.2997	.1848	-54.2
225	.1070	.2913	.1842	-56.3
200	.1012	.2847	.1834	-57.0
175	.0983	.2806	.1822	-56.2
150	.0993	.2789	.1796	-56.3
125	.0980	.2765	.1784	-58.0
100	.0962	.2754	.1792	-60.0
90	.0943	.2745	.1801	-60.7
80	.0914	.2749	.1834	-60.4
70	.0904	.2759	.1855	-60.0
60	.0894	.2775	.1881	-59.6
50	.0867	.2828	.1961	-58.5
40	.0844	.2896	.2052	-57.9
30	.0808	.2977	.2168	-56.9

United States December-January Clear Skies

Pressure	F_{down}	F_{up}	F_{net}	T_{air}
975	.3806	.4653	.0846	-1.9
950	.3684	.4518	.0834	-2.0
925	.3594	.4529	.0935	-1.6
900	.3584	.4546	.0962	-0.9
875	.3612	.4606	.0993	0.0
850	.3510	.4591	.1081	-0.7
825	.3425	.4567	.1141	-1.3
800	.3334	.4527	.1192	-1.9
775	.3250	.4491	.1241	-2.7
750	.3167	.4457	.1289	-3.5
725	.3080	.4430	.1350	-4.4
700	.2994	.4410	.1416	-5.7
675	.2905	.4370	.1465	-7.1
650	.2802	.4322	.1520	-8.8
625	.2698	.4280	.1582	-10.3
600	.2588	.4228	.1639	-12.3
575	.2473	.4170	.1696	-14.3
550	.2361	.4116	.1754	-16.6
525	.2244	.4060	.1815	-18.9
500	.2101	.3987	.1886	-21.5
475	.1964	.3920	.1955	-24.3
450	.1861	.3850	.1989	-27.1
425	.1731	.3775	.2044	-30.0
400	.1624	.3701	.2077	-33.3
375	.1505	.3628	.2122	-36.3
350	.1397	.3560	.2162	-39.6
325	.1302	.3487	.2184	-43.2
300	.1208	.3411	.2202	-47.0
275	.1116	.3345	.2229	-50.5
250	.1045	.3269	.2224	-53.9
225	.0988	.3196	.2208	-56.7
200	.0926	.3126	.2199	-58.6
175	.0903	.3066	.2163	-58.9
150	.0892	.3043	.2150	-58.7
125	.0890	.3035	.2144	-59.7
100	.0873	.3005	.2131	-61.5
90	.0854	.2996	.2142	-61.5
80	.0829	.3009	.2172	-61.2
70	.0808	.3044	.2235	-60.8
60	.0789	.3058	.2268	-60.3
50	.0761	.3101	.2339	-59.3
40	.0743	.3149	.2405	-59.2
30	.0695	.3196	.2501	-58.2

United States December-January Low and Middle Clouds Overcast

Pressure	F_{down}	F_{up}	F_{net}	T_{air}
975	.4813	.5097	.0284	1.6
950	.4478	.4785	.0307	-2.0
925	.4335	.4667	.0331	-2.5
900	.4224	.4605	.0380	-2.2
875	.4151	.4567	.0415	-2.1
850	.4086	.4539	.0453	-2.6
825	.4004	.4512	.0507	-3.3
800	.3902	.4482	.0580	-4.0
775	.3799	.4445	.0645	-4.8
750	.3705	.4399	.0694	-5.9
725	.3610	.4348	.0737	-7.3
700	.3503	.4295	.0791	-8.6
675	.3391	.4247	.0855	-10.0
650	.3291	.4190	.0898	-11.6
625	.3192	.4132	.0939	-13.4
600	.3059	.4061	.1001	-15.2
575	.2938	.3994	.1056	-17.2
550	.2827	.3921	.1093	-19.3
525	.2722	.3837	.1115	-21.4
500	.2599	.3747	.1147	-24.0
475	.2452	.3652	.1199	-26.6
450	.2283	.3554	.1270	-29.1
425	.2134	.3460	.1326	-31.8
400	.1990	.3366	.1376	-34.8
375	.1825	.3271	.1445	-37.9
350	.1652	.3177	.1523	-41.2
325	.1491	.3094	.1603	-44.7
300	.1358	.3005	.1646	-47.7
275	.1249	.2928	.1679	-50.2
250	.1178	.2828	.1649	-52.3
225	.1122	.2769	.1647	-53.2
200	.1069	.2739	.1670	-54.4
175	.1048	.2702	.1654	-54.0
150	.1052	.2692	.1639	-55.9
125	.1028	.2624	.1595	-58.8
100	.0983	.2627	.1644	-61.2
90	.0959	.2632	.1672	-63.3
80	.0912	.2616	.1703	-62.8
70	.0898	.2624	.1726	-62.0
60	.0895	.2680	.1784	-61.7
50	.0873	.2753	.1879	-60.3
40	.0837	.2840	.2003	-59.4
30	.0797	.2972	.2175	-59.3

United States December-January Cirrus Overcast

Pressure	F_{down}	F_{up}	F_{net}	T_{air}
975	.4283	.4981	.0698	2.5
950	.4196	.4920	.0724	2.2
925	.4132	.4879	.0746	3.0
900	.4087	.4843	.0756	3.6
875	.4121	.4915	.0795	5.3
850	.4034	.4909	.0875	4.5
825	.3941	.4873	.0932	3.3
800	.3851	.4851	.1000	2.1
775	.3754	.4804	.1051	1.0
750	.3661	.4766	.1105	-0.1
725	.3566	.4724	.1158	-1.4
700	.3476	.4682	.1206	-2.6
675	.3389	.4628	.1238	-3.9
650	.3302	.4574	.1272	-5.6
625	.3222	.4514	.1293	-7.4
600	.3136	.4458	.1322	-9.5
575	.3042	.4388	.1346	-11.7
550	.2930	.4318	.1388	-14.0
525	.2829	.4243	.1414	-16.5
500	.2701	.4155	.1454	-19.1
475	.2596	.4073	.1477	-21.7
450	.2476	.3975	.1499	-24.8
425	.2351	.3885	.1533	-28.0
400	.2216	.3752	.1536	-31.5
375	.2081	.3631	.1550	-35.3
350	.1893	.3482	.1589	-39.1
325	.1720	.3329	.1608	-43.3
300	.1507	.3174	.1667	-47.9
275	.1352	.3032	.1680	-52.4
250	.1181	.2872	.1692	-57.1
225	.1033	.2741	.1707	-60.8
200	.0938	.2592	.1654	-62.2
175	.0883	.2505	.1622	-60.8
150	.0898	.2487	.1588	-59.2
125	.0892	.2505	.1613	-59.6
100	.0872	.2550	.1678	-61.0
90	.0859	.2555	.1696	-61.9
80	.0851	.2529	.1678	-61.6
70	.0839	.2538	.1699	-61.5
60	.0821	.2543	.1722	-60.8
50	.0822	.2552	.1730	-60.0
40	.0778	.2599	.1821	-59.0
30	.0739	.2640	.1902	-58.1

Caribbean December-January All Ascents

Pressure	F_{down}	F_{up}	F_{net}	T_{air}
1000	.6054	.6618	.0564	24.3
975	.5864	.6546	.0681	22.1
950	.5721	.6474	.0752	20.2
925	.5550	.6377	.0826	18.6
900	.5384	.6277	.0893	17.1
875	.5224	.6175	.0951	15.7
850	.5060	.6087	.1026	14.4
825	.4896	.5998	.1101	13.2
800	.4726	.5913	.1186	11.9
775	.4563	.5837	.1273	10.6
750	.4386	.5755	.1368	9.4
725	.4220	.5686	.1465	8.3
700	.4063	.5625	.1561	7.0
675	.3900	.5562	.1661	5.8
650	.3744	.5490	.1746	4.4
625	.3601	.5418	.1817	2.8
600	.3464	.5351	.1887	0.9
575	.3326	.5279	.1953	-0.8
550	.3190	.5205	.2015	-3.0
525	.3053	.5131	.2078	-5.2
500	.2907	.5046	.2139	-7.6
475	.2767	.4962	.2195	-10.1
450	.2614	.4867	.2253	-13.2
425	.2475	.4783	.2308	-16.3
400	.2341	.4687	.2346	-19.6
375	.2195	.4582	.2386	-23.1
350	.2059	.4483	.2424	-26.8
325	.1929	.4372	.2442	-31.1
300	.1784	.4256	.2472	-35.7
275	.1625	.4127	.2501	-40.4
250	.1462	.3985	.2522	-45.6
225	.1304	.3867	.2563	-50.9
200	.1163	.3740	.2576	-56.4
175	.1060	.3604	.2544	-61.6
150	.0971	.3517	.2546	-65.6
125	.0923	.3444	.2521	-70.5
100	.0847	.3460	.2612	-76.8
90	.0824	.3439	.2615	-78.6
80	.0795	.3490	.2695	-78.6
70	.0770	.3502	.2731	-75.4
60	.0772	.3569	.2796	-70.0
50	.0807	.3638	.2831	-65.2
40	.0838	.3741	.2902	-62.6
30	.0858	.3828	.2969	-59.6

Caribbean December-January Clear Skies (1/10 Cumulus)

Pressure	F_{down}	F_{up}	F_{net}	T_{air}
1000	.6034	.6653	.0618	25.0
975	.5812	.6572	.0760	22.9
950	.5648	.6517	.0869	20.9
925	.5462	.6426	.0964	19.3
900	.5280	.6333	.1053	17.9
875	.5116	.6234	.1118	16.5
850	.4943	.6146	.1203	15.1
825	.4757	.6050	.1292	13.8
800	.4578	.5971	.1393	12.5
775	.4417	.5904	.1487	11.3
750	.4245	.5815	.1570	10.1
725	.4066	.5737	.1670	9.1
700	.3906	.5675	.1769	8.0
675	.3765	.5624	.1858	6.9
650	.3619	.5568	.1948	5.5
625	.3479	.5504	.2024	3.8
600	.3339	.5442	.2102	1.8
575	.3190	.5374	.2184	0.0
550	.3052	.5303	.2250	-2.1
525	.2913	.5229	.2316	-4.4
500	.2771	.5152	.2380	-6.8
475	.2635	.5075	.2440	-9.2
450	.2502	.4990	.2488	-12.1
425	.2374	.4916	.2542	-15.3
400	.2242	.4825	.2582	-18.5
375	.2108	.4725	.2616	-22.1
350	.1976	.4635	.2659	-25.8
325	.1841	.4527	.2685	-30.2
300	.1699	.4417	.2718	-34.9
275	.1550	.4293	.2743	-39.7
250	.1403	.4162	.2758	-44.8
225	.1267	.4049	.2782	-50.1
200	.1138	.3927	.2788	-55.5
175	.1043	.3813	.2769	-61.2
150	.0949	.3729	.2780	-65.7
125	.0902	.3647	.2744	-71.2
100	.0833	.3624	.2790	-77.6
90	.0810	.3585	.2775	-79.2
80	.0790	.3558	.2767	-79.0
70	.0768	.3540	.2772	-75.8
60	.0769	.3625	.2855	-69.9
50	.0808	.3702	.2893	-65.1
40	.0843	.3764	.2921	-62.2
30	.0866	.3874	.3007	-59.1

BIBLIOGRAPHY

Brooks, D. L., 1958: The distribution of carbon dioxide cooling in the lower stratosphere. Journal of Meteorology, 15, 210-219.

Bushnell, R. H., Suomi, V. E., 1961: Experimental flight verification of the economical net radiometer. J. Geophys. Research, 66, 9, 2843-2848.

Bushnell, R. H., 1962: Personal communication with the author.

Darkow, G. L., 1960: Infrared radiation measurements near the tropopause, Annual Report, Contract CWB 9757, Department of Meteorology, University of Wisconsin.

Davis, P. A., 1961: A re-examination of the heat budget of the troposphere and lower stratosphere, Report Number 3, Contract Af 19 (604) - 6146. Research Division, College of Engineering, New York University.

Elsasser, W. M., 1942: Heat transfer by infrared radiation in the atmosphere. Harvard Meteor. Studies, No. 6, Cambridge, Harvard Univ. Press, 107 pp.

Goody, R. M., 1949: The thermal equilibrium at the tropopause and the temperature of the lower stratosphere. Proceeding of the Royal Society of London, A, 197, 1949, pp. 487-505.

Goody, R. M., 1954: The Physics of the Stratosphere. Cambridge, England, Cambridge Univ. Press, 87 pp.

Korb, G., Michelowsky, J., and Moller, F., 1957: Investigation of the heat balance of the troposphere, Technical Report Number 2, Contract AF 61(514)-1005, Johannes Gutenberg-Universitat. Meteorologisch-Geophysickalisches Institut.

Kuhn, P. M., 1961: Accuracy of the airborne Net Radiometer, Monthly Weather Review, August, 1961.

Kuhn, P. M., 1962: Personal communication with the author.

Kuhn, P. M., V. E. Suomi, G. L. Darkow, 1959: Soundings of terrestrial radiation flux over Wisconsin, Monthly Weather Review, 87, 129, April, 1959.

Kuhn, P. M., and V. E. Suomi, 1960: Infrared radiometer soundings on a synoptic scale. Journal of Geophysical Research, 65, 3669-3677.

London, J., 1952: The distribution of radiational temperature change in the northern hemisphere during March. Geophysical Research Papers, Number 18, Geophysics Research Directorate, 64 pp.

London, J., 1956: The heat balance of the atmosphere. Final Report, Contract Number AF 19(122)-165. Research Division, Department of Meteorology and Oceanography, College of Engineering, New York University.

London, J., 1957: A study of the atmospheric heat balance. Final Report, Contract Number AF 19(122) - 165. Research Division, College of Engineering, New York University.

London, J., Ohring, G., and Ruff, I., 1956: Radiative properties of the stratosphere. Final Report, Contract Number AF 19(604) - 1285. Research Division, Department of Meteorology and Oceanography, College of Engineering, New York University.

Moller, F., 1956: The pattern of radiative heating and cooling in the troposphere and lower stratosphere. Proceedings of the Royal Society of London, A, 236, 148-156.

Moller, F., 1959: Radiation and Meteorology, Paper presented at the meeting of the Radiation Commission of IAMAP. Oxford, 20 July 1959.

Manabe, S., Moller, F., 1961: On the radiative equilibrium and heat balance of the atmosphere, Monthly Weather Review, Vol. 89, No. 12, December, 1961.

Plass, G. N., 1956: The influence of the 9.6 micron ozone band on the atmospheric infrared cooling rate. Quarterly Journal of the Royal Meteorological Society, v. 82, pp. 30-44.

Plass, G. N., 1956: The influence of the 15μ carbon dioxide band on the atmospheric infrared cooling rate, Quarterly Journal of the Royal Meteorological Society, vol. 82, No. 353, July 1956, pp. 310-324.

Ohring, G., 1958: The radiation budget of the stratosphere. Journal of Meteorology, 15, 440-451.

Sabatini, R. R., and Suomi, V. E., 1962: On the possibility of atmospheric infrared cooling estimates from satellites. Submitted for publication.

Suomi, V. E., Kuhn, P. M., 1958: An economical net radiometer, Tellus, Vol. 10, Number 1.

Krishnamurti, T. N., 1961: The subtropical jet stream of winter. Journal of Meteorology, 18, 172-191, April, 1961.

Staley, D. O., 1958: Some comments on physical processes at and near the tropopause. Arch. Met. Geoph. Biokl. A, Bd. 10, H1, 1958.